Ozone and onions

How excess UV-B radiation
can damage plants

Are food preservatives toxic?
Investigating potentially harmful effects of common products

Let there be light
How bioluminescence measurements could help clear infections

Pollen desensitization therapy
Can ingestion of pollen products help people suffering from allergies?

Pollution prevention
Evaluating the performance of graphene oxide filters

JOURNAL OF
EMERGING INVESTIGATORS

The Journal of Emerging Investigators is an open-access journal that publishes original research in the biological and physical sciences that is written by middle and high school students. JEI provides students, under the guidance of a teacher or advisor, the opportunity to submit and gain feedback on original research and to publish their findings in a peer-reviewed scientific journal. Because grade-school students often lack access to formal research institutions, we expect that the work submitted by students may come from classroom-based projects, science fair projects, or other forms of mentor-supervised research.

JEI is a non-profit group run and operated by graduate students, postdoctoral fellows, and professors across the United States.

FOUNDING SPONSORS

ALLOY THERAPEUTICS

NEW ENGLAND BioLabs Inc.
enabling technologies in the life sciences

Contents

The non-thermal effect of UV-B irradiation on onion growth

Mohamed Nashnoush, Judy Rodgers

Yarmouth Consolidated Memorial High School, Yarmouth, Nova Scotia

SUMMARY

Both terrestrial and aquatic plants, the chief autotrophs supporting life on earth, can be threatened by global warming and particularly by UV-B radiation due to the depletion of the ozone layer. Ozone depletion may also threaten the biodiversity of ecosystems and dismantle food webs. The deleterious effects of UV-B have been studied mostly through *in vitro* studies and vary significantly according to the dose received, the irradiation period and the sensitivity of the species. Examined adaptive mechanisms encompass increases in antioxidant enzymes, phenolic compounds and flavonoids which function as protective screens. The interaction of UV-B radiation with DNA, lipid and protein molecules is vital in determining how photosynthesis and cellular respiration are affected by UV-B radiation. Hence, this study seeks to explore the non-thermal effects of UV-B irradiation on the physiology and morphology of *Allium cepa*. This was completed by comparing the mitotic index of the control to the irradiated populations. A paired samples two-tailed t-test was performed, and the results demonstrated a decline in mitotic vitality, suggesting that UV-B can generate biochemical stress, which can influence *Allium cepa*'s physiology.

INTRODUCTION

The Montreal Protocol banned the use of chlorofluorocarbons (CFCs) due to ozone layer depletion and increased exposure to harmful short wavelength radiation (1). CFCs disrupt the ozone-oxygen cycle by reacting with radical oxygen atoms, preventing the formation of ozone (1). The "ozone hole" is predicted to be twenty-four million kilometers in diameter, allowing ultraviolet (UV) radiation to penetrate through the troposphere, increasing the exposure of plants and mammals to ionizing radiation (1). There are now plenty of alternatives to the use of volatile CFCs; however, the struggle to completely eliminate this compound continues, as another source has been detected in the region of East Asia (1). Additionally, other volatile substances (e.g. sulphur oxides, nitrogen oxides, methane and organohalogens) have been found to deplete ozone levels (2). This calls on the need to explore the possible ramifications resulting from UV-B rays penetrating the stratosphere and interacting with crops (2). Onions' (*A. cepa*) indispensable dietary role and ubiquitous nature inspired their use in this study. Our research seeks to explore how the non-thermal effects of UV-B radiation at

300nm influence the growth of *Allium cepa* after zero, one, two, three, four and five hours of exposure.

There are three different types of UV radiation: UV-C, UV-B, and UV-A. UV-C possesses the highest amount of energy, with a wavelength between 100nm and 290nm (2, 3). This type of UV radiation does not penetrate the ozone layer and, consequently, does not reach the earth's surface (3). On the other hand, only a few UV-B rays with a wavelength between 280nm and 320nm penetrate the ozone layer (3). However, with the gradual ozone depletion at the stratosphere, increasing amounts of UV-B rays are entering (1, 2, 3). UV-A with wavelengths between 320nm and 400nm is considered benign relative to the aforementioned types of UV (3). UV-A mostly penetrates the ozone layer; however, the low amount of energy possessed by UV-A is not sufficient to pose any hazards to plants (3). UV-B was selected for examination in this study, as it is pertinent to both the Permian extinction and contemporary ozone depletion resulting from atmospheric pollutants (3). Further, an average wavelength of 300nm was adopted in the methodology to represent the wavelength segment of UV-B radiation fairly (4).

Work by Reboredo noted that, as a consequence of UV-B ambient irradiation, concentrations of chlorophyll a and chlorophyll b progressively declined (4, 5). Further, pigment degradation increased, and changes in the structure of Rubisco led to a loss in function (6). Thus, levels of photosynthesis are likely to decline, and concentrations of glucose will consequently decrease (6). This will lower the rate of respiration and lead to a reduction in the levels of ATP (6, 7). Reduction in the levels of ATP could lead to a variety of different events. One of the anticipated events would be cells entering G_0 phase, as ATP concentrations are not sufficient to allow Cyclin-dependent kinases to activate all enzymes required to perform roles for a specific stage of the cell cycle (8). Hence, it was hypothesized that the mitotic index would decrease as irradiation time increases.

Our results may be of global significance and could prompt the prevention of volatile substances that may threaten the biodiversity of ecosystems. Comprehending how plants respond to UV-B can allow us to gain a better grasp of the dietary risks associated with the consumption of irradiated varieties and the consequential effects on ecosystems.

RESULTS

To test the hypothesis the onion root tips were grown over a four-week period, where regular hydration, aeration

Figure 1: Experimental set up for growing onion sets. Figure highlights how all onion bulbs are equally spaced to reduce the prospect of intra-specific competition.

and sunlight exposure were conducted **(Figure 1)**. Some *A. cepa* varieties were subject to UV-B irradiation, and a control group was left untreated **(Figure 2)**. Root tips were carefully harvested and were utilized as a marker of cellular proliferation due to the presence of the apical meristem. Requisite raw data was collected to calculate mitotic indices of the irradiated and control groups.

After several weeks, most onion bulbs successfully sprouted. There was a noticeable increase in biomass and an increase in the girth of the shoots. Fortunately, saprotrophic mold did not develop, signaling adequate growth conditions (9). However, after the duration of four weeks, five onion bulbs failed to develop noticeable shoots. This is likely due to the varying ages of onion bulbs, which determines their ability to grow further. This also explains why some onions developed extensive shoots in a few days. Onion root cells within a forty-cell area were noted **(Figure 3)**. Lastly, it was noted after five hours of irradiation, the shoots appeared to sag, suggesting loss of cellular turgidity (9).

The high coefficient of determination (R^2) suggests the data points closely fit the regression line, which indicates that the line of best fit is a reliable illustration of the association between the variables **(Figure 4)**. Additionally, the negative linear trend observed is confirmed by the negative gradient of the equation of the line of best fit ($y=-4.5x+49$). To examine the extent of statistical dependence between the dependent and independent variables, the correlation coefficient (r) was calculated. The correlation coefficient was found to be $r=-0.94$, which suggests there is a strong negative correlation between the variables. Further, there is some overlap between the error bars, which alludes to trivial or non-existing differences between some sample means. Limitations certainly arise from high biological variance, which is indicated by the high standard deviation and standard error values across all samples, as seen in **Table 1.**

To deduce the extent of statistical significance in the data collected, we performed an inferential statistical test as illustrated in **Table 2**. The assumptions made by the paired samples two-tailed t-test were all satisfied by the data collected, which encouraged us to perform this particular

statistical test. These assumptions included normality, continuous nature of the dependent variable, dependence of observations and random sampling, all of which have been satisfied, qualifying the data for this statistical test (10). The t-test was completed to compare two sample means from the same population, indicating if there is a significant statistical difference between the two samples. The results conclusively reveal that only the four- and five-hour groups are statically significant at 95% confidence. This is alluded to and foreshadowed by the substantial difference in the mean mitotic indices of both groups relative to the control. Such reduction in the mitotic vitality is investigated deeper in the discussion section.

DISCUSSION

As seen in the results section, the mean mitotic index decreases as irradiation time increases. This negative trend between the variables is visually represented by the line of best fit in **Figure 4**, which was discovered to be a reliable illustration of the relationship between variables due to the high coefficient of determination ($R^2=0.89$). Further, the negative correlation between the variables is deemed strong by the low correlation coefficient ($r=-0.94$). These results support the aforementioned hypothesis, and hence one can infer that as UV-B irradiation increases, the growth of onions decreases.

The decline in the mean mitotic index is largely due to the harmful effects of UV-B irradiation on the various leaf structures. Namely, UV-B radiation can reduce stomatal conductance by increasing concentrations of Abscisic acid
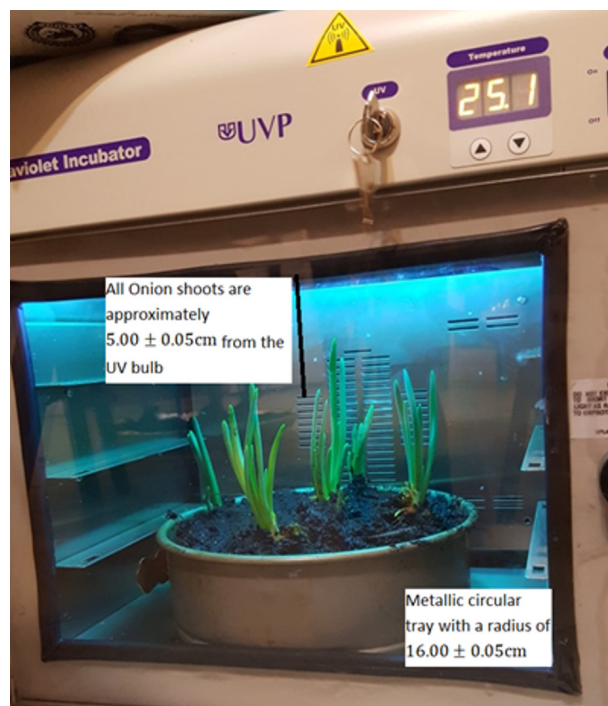

Figure 2: Experimental set up for irradiation of onions. The irradiation setup reveals how all onion shoots receive the same intensity of UV-B rays.
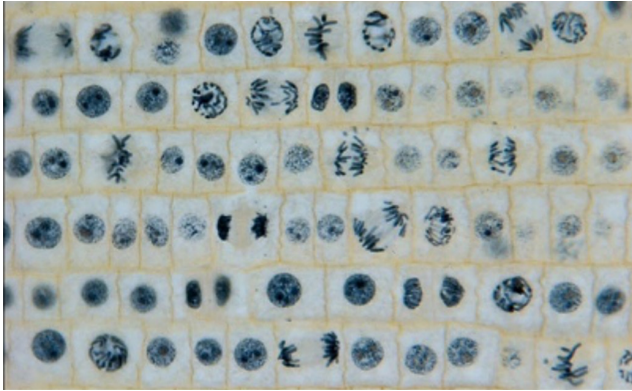
Figure 3: Micrograph of onion root tip. The micrograph of an onion root tip displays a 40-cell parameter, which was achieved at ×40 total magnification.

in the leaves (11). Concentrations of Abscisic acid would accumulate in the leaves due to biochemical stress (6, 9, 11). This could explain why the shoots appeared flaccid after irradiation, as the transpiration rate reached a halt, and negative pressure was no longer generated to mobilize water up the Xylem (11). Further, UV-B irradiation can generate oxyradicals, as oxygen molecules absorb higher amounts of energy carried by UV-B photons forming energetic radicals (6, 7, 11). These oxyradicals substantially inhibit the normal function of growth hormones, such as cytokinins and auxin (11, 12). This is because plant hormones are highly sensitive to photooxidative stress. Additionally, an increase in the activity of enzymes such as cytokinins dehydrogenase that would otherwise be regulated, uncontrollably inactivate cytokinins (12). Such effects would decrease the metabolic rate, as growth hormones would be present in small concentrations. Consequently, the rate of cellular proliferation in the roots would decrease and hence cells would likely enter the quiescent stage of G_0, or in extreme cases, go into cellular senescence (3, 6, 12). This could explain why a reduced number of mitotic cells were observed under the compound light microscope. Future iterations of this experiment should consider the use of flow cytometry techniques to objectively analyze the chemical constituent changes that accompany biochemical stress.

Our research could provide a deeper insight into one of the postulated causes of the Permian extinction, as mass extinction could be due to the increasing irradiation to UV-B and UV-C (1, 2, 12). Geologists and volcanologists have found that during the time of the Permian extinction, volcanoes were highly active, frequently erupting and releasing atmospheric pollutants, which could have thinned or debilitated the ozone layer (2, 11, 13). This would have increased UV exposure levels, and consequently, plants experienced biological stress, which likely led to the collapse of food webs due to a bottom-up factor (1, 2, 13). Populations essentially went extinct because of the dramatically low carrying capacity of the environment. Our study could contribute by outlining the change in the growth patterns accompanying irradiation,

which would provide an indication of what likely happened to various crops present at the time of the Permian extinction.

However, it is important to note that the implications of our research are limited primarily due to our inability to reproduce the natural conditions of the environment. Additionally, limitations arise from high biological variance, which is indicated by the high standard deviation and standard error values across all samples. Due to differences in the genotype, it is very likely that some onions were more acclimated than others to UV-B radiation, which would have led to higher mitotic indices. This is a contributing factor to the high variability seen in the results. Further, as noted qualitatively, the onions had varying abilities to grow, suggesting onions were of different ages, and some may have already reached maturity.

Additionally, the absence of a drainage system and addition of a high volume of distilled water over the duration of four weeks limited our experimental set-up. The effect on onion bulbs is debatable because the container had a high depth. When transplanting, we realized onion bulbs had a tendency to develop lateral roots, as opposed to deep fibrous roots. Thus, it is implausible that aeration of the onions' shallow root network was reduced, as excess water buildup was recorded to occur at a depth of 10cm (i.e. far below the roots). However, adding a high volume of water may have led to leaching of valuable minerals and consequently reduced the potential for growth. This systematic error would reduce the mitotic index across all onions. However, it would not affect the conclusions reached regarding UV-B irradiation as onion samples are compared relative to one another.

It is important to note only 5mL of water was added per day to each onion bulb. This suggests that minimal evaporation occurred and over the span of four weeks; most of the water simply accumulated at the bed of the pots. One solution would be to increase temperatures (e.g. 30°) to evaporate excess water. Another solution is to drill holes in the pots, which will serve as a pathway to enable excess amounts of water to drain out. Further, a saucer can be added underneath to collect excessive amounts of water. The water collected by the saucer can be reused to water the onions, as the water will contain high quantities of dissolved minerals, which through mass flow of water can diffuse passively into the epidermal
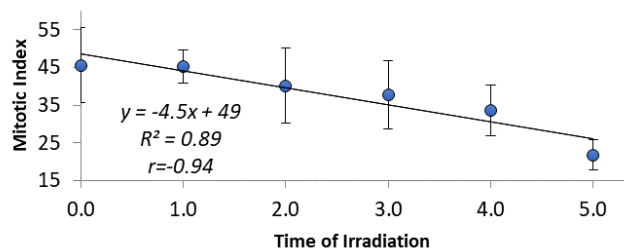

$y = -4.5x + 49$
$R^2 = 0.89$
$r = -0.94$

Figure 4: Mean mitotic indices at varying exposure times. Graphical representation of processed data accentuates the negative association between the variables. Note the vertical error bars were constructed using standard deviation to demonstrate the variability within the data..

Exposure Time	Mitotic indices (%)										
	Trial 1	Trial 2	Trial 3	Trial 4	Trial 5	Trial 6	Trial 7	Trial 8	Mean	Standard Deviation	Standard Error
0.0	36.36	55.17	50.00	42.86	26.53	47.37	46.34	60.53	45.7	9.96	3.8
1.0	53.57	39.47	46.67	41.18	41.03	47.22	44.74	48.65	45.3	4.40	1.7
2.0	26.47	37.50	27.91	37.93	38.98	43.75	51.72	57.14	40.2	9.91	3.7
3.0	44.19	34.38	28.21	23.26	35.29	40.00	42.86	53.85	37.8	9.02	3.4
4.0	39.29	29.41	26.32	25.00	30.30	39.29	33.33	45.83	33.6	6.80	2.6
5.0	21.88	28.57	17.95	16.22	22.45	21.88	26.67	18.75	21.8	3.96	1.5

Table 1: Processed data indicates a consistent decline in the mean mitotic index as the exposure period increases.

cells of the roots. This will reduce the need for the roots to actively pump in various nutrients into the roots and hence direct more of ATP reserves to fulfill growth requirements.

Another limitation is that plants were almost exclusively irradiated with UV-B and consequently, they were deprived of photosynthetically active radiation (PAR). An artificial source of UV-B does not match the diverse solar spectrum of the sun. Several studies have found that the effects of UV-B on vegetative growth and photosynthesis are mitigated by PAR and UV-A radiation (13, 14). For example, it has been found that visible blue light can increase the acclimation of plants by reducing the degradation of photosynthetic pigments (e.g. Chlorophyll a & b and Xanthophylls) and contributing to an increase in the content of protective oils on the epidermis layer (14). This can be rectified by installing a lamp that closely mimics solar radiation, emitting UV-B and PAR rays (e.g. Eye Hortilux PowerVEG T5 H0 Fluorescent Lamp Full Spectrum +UV).

All of these limitations would have led to high standard deviation values, limiting the reliability of the results. However, the standard deviation would be accounted for by the t-test. As seen in **Table 2**, the only two samples shown to be statistically different relative to the control are the 4-hour and 5-hour samples. This suggests that the damage induced by UV-B is not instantaneous and substantiates the mentioned hypothesis. Our findings align with various studies and more importantly, the research provides a supported answer to the research question despite its possible limitations.

Our research does not claim generalizability especially because some native species in high altitudes in the tropics and subtropics have evolved a UV-B sensing protein (UVR8) capable of expressing certain genes, which enable the plant

to release various coating oils serving to protect the plant's leaves (14).

Field-based studies should be conducted to better represent the natural conditions of habitats, which can provide a more realistic indication of the consequences accompanying UV-B irradiation on crops. These field studies should strive to provide a comprehensive picture by considering other parameters (e.g. CO_2 concentration, fluctuations in temperatures, wind speed & topography). Additionally, further research should examine species at high altitudes with adaptive mechanisms, since this can reveal sensitive metabolic pathways. Compounds such as flavonoids, phenolics and anthocyanins, that are released during periods of biochemical stress can be used as biomarkers to detect sensitive areas of a plant (14, 15). Further, more research should be directed towards the regulation of UV-B irradiation at levels where physiological stress is minimized — namely, where irradiation does not present significant growth constraints. This is mainly because UV-B irradiation can increase the synthesis of antioxidants and protective oils, which can increase the medicinal content of crops (14, 15, 16). Additionally, regulated irradiation to UV-B can improve the flavor of some crops and increase the pungency of plant aromas, which may bring benefits to both the food and

		t-statistic	Degrees of Freedom	p-value
Pair 1	Control – 1 hour sample	.082	7	.937
Pair 2	Control – 2 hour sample	1.371	7	.213
Pair 3	Control – 3 hour sample	1.829	7	.110
Pair 4	Control – 4 hour sample	3.083	7	.018
Pair 5	Control – 5 hour sample	5.939	7	.001

Table 2: The statistical results indicate that only variable pair four and five are statistically significant at 95% confidence.

fragrance industries (16). Lastly, different methods should be implemented to measure growth (e.g. dry mass measured by an electronic balance, rate of water absorption recorded by a potometer and use of chromatography techniques to evaluate pigment concentrations). Researchers should also consider elongating irradiation times without completely depriving plants of PAR. This would greatly contribute to our understanding of the effects induced by UV-B irradiation on *Allium cepa*.

MATERIALS AND METHODS
Growing Method

Seven pots with a diameter of 54.0cm and a depth of 11.0cm were first covered using $0.360m^2$ of aluminum foil. Aluminum foil was used to help raise temperatures, as warmth stimulates secretions of various growth hormones (e.g. Auxin) that induce biochemical changes and prompt onions to exit their state of dormancy. Then, loam was added to each pot up to a height of 9.00cm. Eight onions were planted in each pot. When planting, all the tunicated bulbs were buried in the loam such that only the developing shoots project outwards **(Figure 1)**. Further, surrounding each bulb, 7.00g of NPK fertilizer was added. A thermometer was periodically placed into the loam to ensure maintenance of the temperature at 20.0°. Additionally, the humidity of the room was noted every day. Five milliliters of distilled water was added on a daily basis to the loam surrounding each onion shoot. Further, all pots were positioned in close proximity to a transparent window to allow equivalent amounts of sunlight to reach all onion bulbs. Onions were grown for a duration of four weeks to ensure onions had sufficient time to develop roots.

Irradiation and Microscopy Technique

After four weeks, most onions developed apparent shoots, which signaled the development of roots. Five mature onions bulbs were transplanted in a circular tray. The tray already contained loam, which allowed onions to be positioned as if in the natural environment. A ruler was used to ensure the distance between the onion shoots and UV-B light bulb was approximately 5.00cm **(Figure 2)**. Afterwards, the tray was placed in the UVP UV Incubator SI-950, and the incubator door was locked firmly. The temperature was set at 25.0°. Once UV-B irradiation began, the stopwatch was promptly started. After one hour, UV-B irradiation was ceased for a brief moment, and the incubator was opened to carefully remove a single onion bulb, which was then placed on the counter. This was done in one-hour intervals to obtain one-, two-, three-, four-, and five-hour irradiated onions. The maximum irradiation period was limited to only five hours, as a safety hazard is posed by surpassing the five-hour mark (17).

Once an onion bulb was irradiated for the designated period, a metal scalpel was used to carefully cut a segment 1.25cm long from the root tip. A glass rod was then rolled along the length of the root tip to forcefully squash the root tip. Then, 2.00mL of 0.1% Sigma-Aldrich Methylene blue

was dispensed into an Eppendorf tube. The crushed length of the root was then placed in the Eppendorf tube, and the solution was vigorously swirled. After swirling, tweezers were then used to transfer the root tip onto a glass microscope slide. Then, 1.00mL of 0.1% Methylene blue was added to the microscope slide. Subsequently, a microscope coverslip was gently lowered at an angle on the onion root to avoid trapping air bubbles under the coverslip. The sample was then analyzed under a compound light microscope at ×40 total magnification. After the irradiated samples were viewed under the microscope, the control (0 hours) was promptly examined under the microscope. The numbers of mitotic and non-mitotic cells were noted for each sample. Forty-eight samples were examined under a compound light microscope to attain eight trials.

The different stages of the cell cycle were discerned by studying the changes in internal cellular structure accompanying phase transitions. The most apparent indication that cells are undergoing interphase is that the sister chromatids or chromosomes are not visible under a compound light microscope, as supercoiling did not occur yet (18). Further, prophase can be discerned when sister chromatids become visible as a result of supercoiling, and when there is a nuclear envelope encapsulating the visible sister chromatids. In metaphase, the nuclear envelope breaks, and sister chromatids align along the equator where the spindle microtubules attach to the centromeres (18). In anaphase, the centromere breaks, and the sister chromatids are pulled to opposite poles of the cell. Telophase can be recognized by the formation of a nuclear membrane surrounding the newly separated chromosomes, as well as loss of visible chromosomes as a consequence of uncoiling (18, 19). Finally, during cytokinesis, a cell wall forms along the equator, separating the cell into two individual cells. Cells in mitosis (prophase, metaphase, anaphase and telophase) were considered mitotic cells and cells in interphase (G_1, S & G_2) and cytokinesis were deemed non-mitotic cells (19).

Statistics

The Statistical Package for the Social Sciences (SPSS) program produced p-values that were statistically significant at 95% confidence for the 4-hour and 5-hour populations. The remainder of populations were characterized as non-significant based upon the p-values.

To ensure the data met the assumptions of the paired samples t-test, several statistical tests were carried out beforehand. Normality was tested through the application of Normal Q-Q plots, Kolmogorov-Smirnov2 normality tests, Shapiro-Wilk normality test, skewness values and kurtosis values. To test for outliers, a box and whisker plot was utilized. All statistical descriptors were generated using SPSS.

REFERENCES

1. Benca, Jeffrey P., Ivo AP Duijnstee, and Cindy V. Looy. "UV-B–induced forest sterility: Implications of ozone shield failure in Earth's largest extinction." *Science Advances*, vol. 4, no. 2, 2018, pp. 16-3. DOI. 10.1126/sciadv.1700618

2. Caldwell, Martyn M. "Solar UV irradiation and the growth and development of higher plants." *Photophysiology*, vol. 6, no. 1, 1971, pp. 131-177. DOI. 10.1007/BF00349807.

3. Caldwell, M. M., *et al*. "Action spectra and their key role in assessing biological consequences of solar UV-B radiation change." *Stratospheric ozone reduction, solar ultraviolet radiation and plant life,* vol. 6, no. 1, 1986, pp. 87-111. DOI. 10.1039/c0pp90035d

4. Flint, Stephan D., and Martyn M. Caldwell. "A biological spectral weighting function for ozone depletion research with higher plants." *Physiologia plantarum*, vol. 117, no. 1, 2003, pp. 137-144. DOI. 10.1032/BF0383922

5. Reboredo, Fernando, and Fernando JC Lidon. "UV-B radiation effects on terrestrial plants-A perspective." *Emirates Journal of Food and Agriculture*, vol. 1, no. 2, 2012, pp. 502-509. DOI. **doi**.org/10.9755/ejfa.v24i6.14670

6. Jingjing, Xu, *et al*. "Effects of Enhanced UV-Radiation on Morphological and Physiological Characters of Welsh Onion [J]." *Chinese Agricultural Science Bulletin*, vol. 11, no. 2, 2008, pp. 120-134. DOI. 10.1016/**j**.plaphy.2016.04.004

7. Shimotohno, Akie, *et al*. "The plant-specific kinase CDKF; 1 is involved in activating phosphorylation of cyclin-dependent kinase-activating kinases in Arabidopsis." *The Plant Cell*, vol. 16, no. 11, 2004, pp. 2954-2966. DOI. 10.1105/tpc.104.025601

8. Coohill, Thomas P. "Ultraviolet action spectra (280 to 380 nm) and solar effectiveness spectra for higher plants." *Photochemistry and photobiology*, vol. 50, no. 4, 1989, pp. 451-457. DOI. 10.1016/1011-1344(92)80043-u

9. Lidon, Fernando JC, *et al*. "Impact of UV-B radiation on photosynthesis-an overview." *Emirates Journal of Food and Agriculture*, vol. 10, no. 4, 2012, pp. 546-556. DOI. 10.9755/ejfa.v24i6.14673

10. Hsu, Henry, and Peter A. Lachenbruch. "Paired t test." *Wiley encyclopedia of clinical trials*, vol. 1, no. 3, 2007, pp. 345-378. DOI. 10.1155/2014/604581.

11. Vanhaelewyn, Lucas, *et al*. "Hormone-controlled UV-B responses in plants." *Journal of experimental botany*, vol. 67, no. 15, 2016, pp. 4469-4482. DOI. 10.1155/2014/604581.

12. Davies, Peter J. "The plant hormones: their nature, occurrence, and functions." *Plant hormones*, vol. 1, no. 15, 2010, pp. 12-56. DOI. 10.1007/978-1-4020-2686-7_1.

13. Nawkar, Ganesh M., *et al*. "UV-induced cell death in plants." *International journal of molecular sciences*, vol. 14, no. 1, 2013, pp. 1608-1628. DOI. 10.3390/ijms14011608

14. Escobar-Bravo, Rocio, Peter GL Klinkhamer, and Kirsten A. Leiss. "Interactive effects of UV-B light with abiotic factors on plant growth and chemistry, and their consequences for defense against arthropod herbivores." *Frontiers in Plant Science,* vol. 27, no. 8, 2017, pp. 14-45. DOI. 10.1080/15592324.2019.1581560.

15. Kakani, V. G., *et al*. "Field crop responses to ultraviolet-B radiation: a review." *Agricultural and forest meteorology,* vol. 120, no. 4, 2003, pp. 191-218. DOI. 10.1016/j.agrformet.2003.08.015

16. Kataria, Sunita, Anjana Jajoo, and Kadur N. Guruprasad. "Impact of increasing Ultraviolet-B (UV-B) radiation on photosynthetic processes." *Journal of Photochemistry and Photobiology B: Biology,* vol. 137, no. 1, 2014, pp. 55-66.

17. Xiong, Fusheng S., and Thomas A. Day. "Effect of solar ultraviolet-B radiation during springtime ozone depletion on photosynthesis and biomass production of Antarctic vascular plants." *Plant Physiology,* vol. 125, no. 2, 2001, pp. 738-751. DOI. 10.1104/pp.125.2.738

18. Rozema, J., *et al*. "The role of UV-B radiation in aquatic and terrestrial ecosystems—an experimental and functional analysis of the evolution of UV-absorbing compounds." *Journal of Photochemistry and Photobiology B: Biology,* vol. 66, no. 1, 2002, pp. 2-12. DOI. 10.1029/2002PA000853.

19. González-Fernández, A., *et al*. "A model for dynamics of cell division cycle in onion roots." *Protoplasma,* vol. 65, no. 3, 1968, pp. 263-276. DOI. 10.1104/pp.116.4.151

Elucidating the genotoxicity of synthetic food preservatives with the SOS chromotest

Kris V. Shah, Conrad Rogers
Harry D. Jacobs High School, Algonquin, Illinois

SUMMARY

The increased use of synthetic food preservatives makes it imperative to screen for their potential health risks. This project aimed to delineate the genotoxic potential and effects of commonly used synthetic food preservatives, specifically sodium nitrite, potassium sulfate, and hydrogen peroxide. We employed a colorimetric assay designed to test the induction of the DNA damage response using beta-galactosidase (β-gal) as a reporter. Evidence suggests these food preservatives may be genotoxic due to their ability to impair normal cellular pathways. We hypothesized that sodium nitrite would be the most genotoxic because nitrites are precursors to *N*-nitrosamines, a class of compounds that are carcinogenic byproducts of metabolism. Potassium sulfate and hydrogen peroxide were also initially hypothesized to be genotoxic. Two-fold serial dilutions were performed, and blue color formation was analyzed qualitatively and quantitatively to assess genotoxicity levels. The hypotheses were partially supported as all synthetic food preservatives demonstrated some degree of genotoxicity before and after metabolic activation; potassium sulfate was shown to be the most genotoxic. The inclusion of mammalian hepatic enzymes permitted for better correlation to humans, as results provided insight on the genotoxicity of food preservatives after normal metabolic function. These findings can inform future toxicology research to potentially prevent genetic damage and carcinogenesis.

INTRODUCTION

The use of synthetic food preservatives continues to grow as preservation techniques become more advanced. As such, it is crucial that certain chemicals and compounds in food are screened for deleterious effects. There has been recent controversy regarding the effects of such chemicals, which warrants questions over their continued use (1). By using the SOS Chromotest assay, the potential genotoxic effects of widely used food preservatives, specifically sodium nitrite, potassium sulfate, and hydrogen peroxide can be effectively evaluated, revealing information that may help to ensure the well-being of consumers and resolve discrepancies in current literature (2, 3). The addition of the rat liver S9 fraction can further characterize any genotoxic effects that may become apparent through this assay (4).

The property of a chemical to cause damage to a cell's DNA is known as genotoxicity. Genotoxic damage can induce mutations, lead to cancer formation, or initiate other human diseases (5). Genotoxins can also cause oxidative damage in which reactive oxygen species (ROS) oxidize the nitrogenous bases, causing the DNA to become unstable. Oxidative damage can result in single-strand and double-strand DNA breaks as well (6).

If damage caused by genotoxic chemicals is not naturally repaired, multiple types of mutations, or permanent changes to a cell's DNA, can occur. Mutations are primarily classified as point or frameshift (7). As mutations accumulate, proteins controlling the rate at which a cell divides may be produced abnormally. This can initiate carcinogenesis, the formation of tumors that have the ability to become cancerous. Mutations can disrupt the normal outcome of many cell signaling pathways. Most tumors are benign and remain restricted to the area they originated, but as some grow and further mutate, they can become malignant and metastasize to other tissues (8).

Sodium nitrite ($NaNO_2$) is a compound used abundantly in the meat industry during the process of curing to prevent microbial growth. When meats containing sodium nitrite are consumed, *N*-nitroso compounds (NOCs) are formed through the process of nitrosation, as nitrites combine with natural amines to form nitrosamines. Previous literature has linked red meat cured with nitrites to gastrointestinal cancer and glioma (9, 10). Nitrates and nitrites are suspected to play a role in the formation of cancers as they are precursors to NOCs. Nitrosamines are also strong neuro-carcinogens in many animal models (3).

Potassium sulfate (K_2SO_4) is another common food preservative used as an anti-browning agent and antioxidant. It is mostly found in dried fruits, vegetables, and sodas; more recently, it has been introduced into cosmetics and medicine. Sulfate exposure was shown to cause health problems such as dermatitis, abdominal pain, and asthmatic symptoms (11). A 2005 study found that sulfate can cause mitotic inhibition and increased the frequency of abnormal mitosis rates, indicating a possible link between sulfate intake and DNA damage (2).

Hydrogen peroxide (H_2O_2) is commonly used to preserve the sweetness of milk. One method of milk preservation consists of using hydrogen peroxide and catalase to reduce souring. Often, catalase does not degrade hydrogen peroxide completely and traces of hydrogen peroxide have been

discovered in dairy products. Because this technique is used for the distribution of milk globally, it is important that its components are screened for genotoxicity. Comet assays performed in a previous study discovered that hydrogen peroxide increased damaging capacity to human hepatoma cells (12). This indicates hydrogen peroxide is a driver of oxidative stress and potential genotoxic compound.

Taking into account the recent health concerns regarding synthetic food preservatives and their correlation with causing adverse health effects, we had the goal of elucidating the genotoxic potential of the food preservatives sodium nitrite, potassium sulfate, and hydrogen peroxide. We also incorporated a novel technique to qualitatively and quantitatively assess genotoxicity levels that would improve connections in our findings to human beings. Including hepatic enzymes would better replicate *in vivo* conditions and replicate the repair systems of humans more closely (12).

All three food preservatives were genotoxic. Genotoxicity levels of sodium nitrite significantly increased after metabolic activation, and the bacteria were able to survive after hydrogen peroxide was metabolized, indicating genotoxicity effectively increased with metabolic activation. Potassium sulfate did not have major differences before and after incorporation of metabolic enzymes as initially predicted. This study demonstrates a potential health risk posed by the consumption of these food preservatives and suggests further evaluation before continued use.

RESULTS
Understanding the SOS Chromotest and SOS response
The human body has various self-repair mechanisms that act to combat different types of DNA damage. These mechanisms are collectively termed, the "DNA damage response (DDR)." DDR detects DNA lesions to promote repair (13). While the SOS box and associated proteins are not present in humans, understanding the SOS system can provide insight on how DDR pathways function. It also serves as a control for determining how chemicals impact the body. The SOS box is a 20-nucleotide long sequence present within the promoter region of genes. The SOS response plays a significant role in the detection of genotoxic substances and subsequent expression of DDR proteins. The LexA protein, which is abundant in prokaryotic cytosols, is a repressor that binds to repress the transcription of SOS-induced proteins. Under normal conditions, LexA can bind the SOS box, functioning as a repressor of SOS-induced proteins. On the other hand, when a cell incurs DNA damage, LexA is cleaved by RecA. Cleaved LexA is unable to bind the SOS box allowing RNA polymerase access to the promoter regions of DNA repair genes, synthesizing repair proteins (14).

The SOS Chromotest uses the activation of genes in the SOS response to detect genotoxicity. It incorporates a strain of *Escherichia coli* in which the LacZ gene is placed under the control of the s*fi*A promoter. LacZ is responsible for the production of β-gal and s*fi*A is the first promoter in the SOS

response. When the *de novo* synthesis of β-gal occurs (as a result of DNA damage), β-gal degrades the lactose analog, X-gal, and an intense blue color is formed providing visual, colorimetric results as a measure of genotoxicity levels. This is then used as a basis for calculating the SOS inducing potency (SOSIP), a linear, universal parameter which measures a cell's ability to induce the SOS response. Based on the β-gal formation and cleavage of X-gal, a dose responsive curve should be attained with positive results.

The SOS Chromotest may confirm uncertainties from other assays such as the Ames test, a widely utilized method for evaluating mutagenic potential. For example, due to its higher sensitivity, the SOS Chromotest has revealed many genotoxic compounds that have been rejected as mutagenic in the Ames test. However, this increased sensitivity has also led to a greater number of false positives (15).

Many genotoxins are activated after being metabolized. For this reason, the SOS Chromotest can be augmented with the addition of the rat liver S9 fraction. S9 contains both cytosol and microsomes which mimic mammalian hepatic metabolism *in vivo*. By using S9, the genotoxicity of a compound before and after natural metabolism can also be assessed. The use of S9 in toxicity assays has previously revealed the genotoxicity of thousands of chemicals that require metabolic activation (4).

Genotoxicity evaluation before metabolism
In order to assess the genotoxicity prior to metabolic processes, the SOS Chromotest was performed without the inclusion of the S9 fraction. This data collected is the baseline control measurement. The experimental set up of the 96-well plate included the respective concentrations, ranging from 3.000% to 0.016% w/w, reagents for controls (sterility, negative, and positive) and three test samples (sodium nitrite, potassium sulfate, and hydrogen peroxide) (**Table 1**). The SOS Chromotest also included the use of 4-nitroquinoline 1-oxide (4NQO) and 2-aminoanthracene (2AA) as positive controls. Incubation time for the plates was a total of three hours. We expected these known genotoxins would develop a deep blue color at high concentrations that would gradually fade as concentrations decreased. 2AA requires metabolic activation to show genotoxic capabilities, therefore it will only follow this pattern after inclusion of the S9 fraction (12). A darker blue color intensity indicates the degradation of X-gal by β-gal, signifying that the SOS response was triggered and DNA damage occurred. After the results were photographed (**Figure 1**), a number value between 1 and 7 was assigned to the positive control wells (4NQO) for the blue color density (1 being the lightest and 7 being the darkest) and a number value of 0 was assigned to the negative control column wells (**Table 2**). The sterility control was performed to ensure the food preservatives did not affect the reagents in the SOS Chromotest. Sterility control wells did not have color development, indicating the assay functioned as expected. Based on the color intensity correlation with the sterility,

	1	2	3	4	5	6	7	8	9	10	11	12
Conc. Level	Negative Control	Positive Control (4NQO)	Positive Control (2AA)	Sodium Nitrate (NaNO$_2$) 3%			Potassium Sulfate (K$_2$SO$_4$) 1%			Hydrogen Peroxide (H$_2$O$_2$) 3%		
				20 µL	10 µL	5 µL	20 µL	10 µL	5 µL	20 µL	10 µL	5 µL
1	100 µL E. coli	100.000%	100.000%	3.000%	3.000%	3.000%	1.000%	1.000%	1.000%	3.000%	3.000%	3.000%
2	100 µL E. coli	50.000%	50.000%	1.500%	1.500%	1.500%	0.500%	0.500%	0.500%	1.500%	1.500%	1.500%
3	100 µL E. coli	25.000%	25.000%	0.750%	0.750%	0.750%	0.250%	0.250%	0.250%	0.750%	0.750%	0.750%
4	100 µL E. coli	12.500%	12.500%	0.375%	0.375%	0.375%	0.125%	0.125%	0.125%	0.375%	0.375%	0.375%
5	100 µL E. coli	6.250%	6.250%	0.188%	0.188%	0.188%	0.063%	0.063%	0.063%	0.188%	0.188%	0.188%
6	100 µL E. coli	3.125%	3.125%	0.094%	0.094%	0.094%	0.031%	0.031%	0.031%	0.094%	0.094%	0.094%
7	100 µL E. coli	1.563%	1.563%	0.047%	0.047%	0.047%	0.016%	0.016%	0.016%	0.047%	0.047%	0.047%
	10 µL DMSO	10 µL 4NQO	10 µL 2AA	100 µL NaNO$_2$	100 µL NaNO$_2$	100 µL NaNO$_2$	100 µL K$_2$SO$_4$	100 µL K$_2$SO$_4$	100 µL K$_2$SO$_4$	100 µL H$_2$O$_2$	100 µL H$_2$O$_2$	100 µL H$_2$O$_2$

Table 1: SOS Chromotest Experimental Design. Each plate included the specific reagents listed in each well and all concentrations are listed in w/w. The second experiment also included the addition of the S9 fraction. Two-fold serial dilutions beginning with the initial concentrations at the top of the columns allowed for the maximum range of concentrations to be tested. Concentration levels are utilized to report concentrations in a uniform manner across the three samples. Each food preservative had three different testing volumes (20 µL, 10 µL, and 5 µL) of the same concentration of sample pipetted into each well.

negative, and positive controls, test sample wells were assigned a number value between -1 and 7 (**Table 2**). A score of -1 signified the bacteria experienced acute toxicity and did not have normal β-gal production, while a score of 0 meant the bacteria survived but remained unharmed.

Genotoxicity evaluation using a metabolism model

The second plate was set up with identical concentrations of reagents and test samples as described above (**Table 1**), but also included the S9 fraction. This would reveal any potential food preservatives that were genotoxic after metabolic activation. The same controls were included in this experiment to ensure the S9 did not interfere with the assay. After the completion of the SOS Chromotest (**Figure 2**), the same scoring methodology was applied as previously done except the 2AA positive control wells were scored instead of the 4NQO wells (**Table 3**). The experimental wells were also scored based on their blue color intensities (**Table 3**) as done in the initial plate.

Figure 1: SOS Chromotest (without S9) Experimental Results. The image depicts the plate against a black background for the genotoxicity evaluation before metabolism. Individual rows and columns are separated based on reagents in each well. Concentrations for each coordinate correspond to those listed in Table 1.
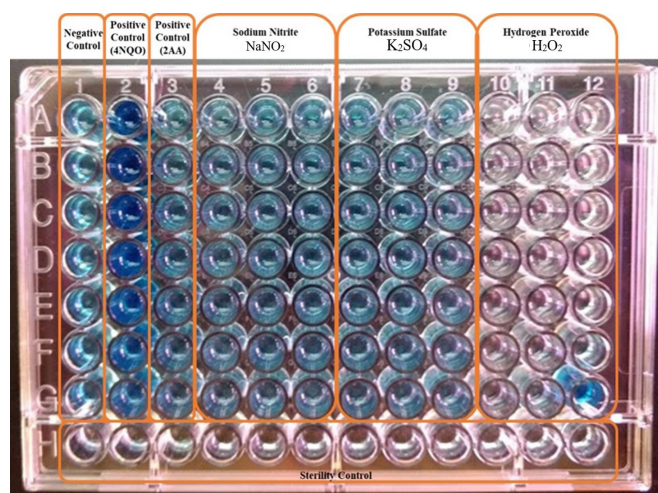

Figure 2: SOS Chromotest (with S9) Experimental Results. The image depicts the plate against a black background for the genotoxicity evaluation after the metabolism model. Individual rows and columns are separated based on reagents in each well. Concentrations for each coordinate correspond to those listed in Table 1.
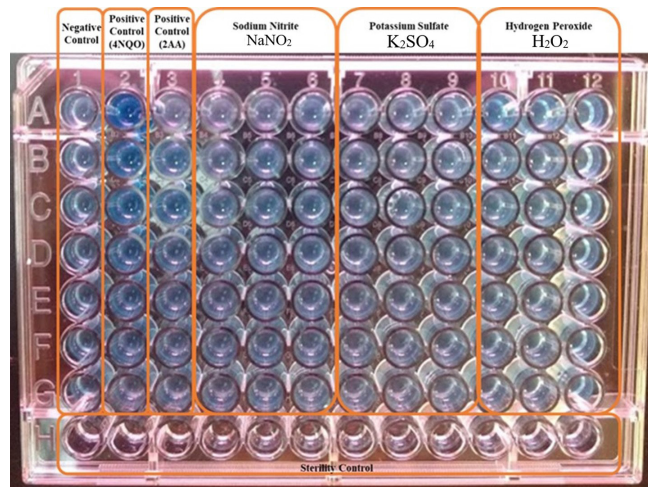
	1	2	4	5	6	7	8	9	10	11	12
Conc. Level	Negative Control	Positive Control (4NQO)	Sodium Nitrate (NaNO$_2$) 3%			Potassium Sulfate (K$_2$SO$_4$) 1%			Hydrogen Peroxide (H$_2$O$_2$) 3%		
			20 µL	10 µL	5 µL	20 µL	10 µL	5 µL	20 µL	10 µL	5 µL
1	0	7	0	1	1	1	0	0	-1	-1	-1
2	0	6	0	1	1	1	1	1	-1	-1	-1
3	0	5	0	1	2	2	2	1	-1	-1	-1
4	0	4	0	1	2	2	2	1	-1	-1	-1
5	0	3	0	1	2	2	2	1	-1	-1	-1
6	0	2	0	1	1	1	1	1	-1	-1	-1
7	0	1	0	0	0	0	0	0	-1	-1	3

Table 2: SOS Chromotest (without S9) Color Intensity Scores. Numerical scores ranged from -1 to 7 based on the positive (4NQO), negative, and sterility controls. The 2AA control was not utilized as the S9 fraction had not been added into this experiment. Initial concentrations are listed in w/w.

Evaluation of results

Analysis of the genotoxic activity of the tested food preservatives can be carried out visually or by using photometric instrumentation (15). A plate reader could not be accessed during this investigation, so the SOSIP could not be calculated. However, numerical assignments were taken to provide quantitative data. Most data was collected and analyzed qualitatively based on blue color formation.

Images of both plates (**Figures 1 & 2**) do not appropriately convey blue color development in the wells, making it difficult to delineate between positive and negative results using only the photographs. Though these results may appear difficult to discern, this is an artifact of the images themselves. Positive results were more apparent during in-person analysis. All numbers for the visual semi-quantitative method for analyzing results were assigned based on color developments observed in-person against both a black and white background. Intensity values against both the black and white backgrounds were averaged and then assigned for final analysis.

Light color development in the negative control containing only *E. coli* was expected as a result of the LacZ::S*fi*A fusion. To visualize numerical assignments, data were plotted in a line graph (**Figures 3 & 4**). This linear comparison is similar to that achieved from the SOSIP and helps analyze a potential dose responsive curve associated with levels of chronic genotoxicity.

Both positive controls (4NQO and 2AA) functioned as expected. While the color change in the 2AA column was notably of less magnitude compared to that of the 4NQO column, this was expected because 2AA is a weaker genotoxic compound (16). The S9 fraction metabolized the test samples and revealed genotoxicity because visual analysis demonstrated a dose responsive curve in the 2AA sample only in the second experiment (**Figure 2**). While S9 seemed to reduce genotoxicity of the 4NQO (**Figure 2**), results cannot be compared between the experiments due to the inherent variability of the SOS Chromotest procedure. Additionally, some cofactors in the S9 mixture may have interfered or diluted the 4NQO solution upon mixing, reducing the color change (16).

Sodium nitrite displayed low levels of genotoxicity before metabolic activation as wells in which 10 µL and 5 µL of the samples were added showed low color development (**Table 2**). Lower concentration was correlated with genotoxicity, reaching a score of 2 for concentrations between 0.188% and 0.750% at a volume of 5 µL of sample (**Figure 3**). At lower concentrations, the genotoxic activity decreased. After metabolic activation, the genotoxicity levels significantly increased at all concentrations for all testing volumes.

	1	3	4	5	6	7	8	9	10	11	12
Conc. Level	Negative Control	Positive Control (2AA)	Sodium Nitrate (NaNO$_2$) 3%			Potassium Sulfate (K$_2$SO$_4$) 1%			Hydrogen Peroxide (H$_2$O$_2$) 3%		
			20 µL	10 µL	5 µL	20 µL	10 µL	5 µL	20 µL	10 µL	5 µL
1	0	7	0	1	3	1	1	1	5	4	2
2	0	6	1	2	3	1	1	1	3	3	2
3	0	5	2	2	4	1	2	2	3	3	2
4	0	4	3	3	4	2	2	2	2	2	2
5	0	3	3	3	2	0	2	1	1	1	0
6	0	2	3	3	2	0	0	0	0	0	0
7	0	1	3	3	0	0	0	0	0	0	0

Table 3: SOS Chromotest (with S9) Color Intensity Scores. Numerical scores were given using the same methodology as Table 2. The 2AA column was used as the positive control instead of 4NQO, as the S9 fraction was included in this experiment. Initial concentrations are listed in w/w.
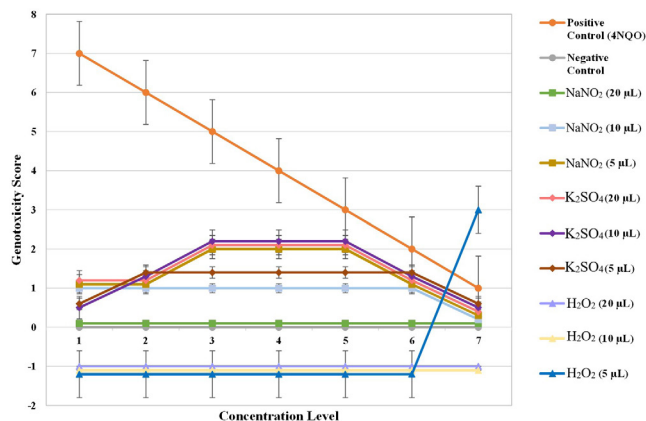
Figure 3: SOS Chromotest (without S9) Genotoxicity Scores. The scores from Table 2 were plotted against concentration level. Concentrations were independent of volume of sample added into each well (20 μL, 10 μL, and 5 μL). Concentrations (in w/w) are consistent with those in Table 1. Dose responsive curve is not evident in comparison to the positive control (4NQO).
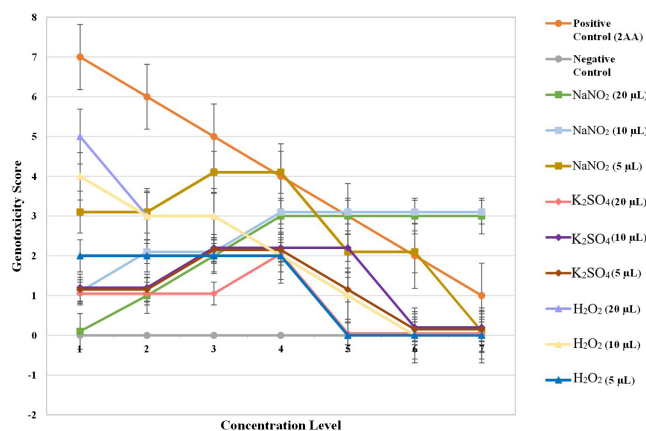

Figure 4: SOS Chromotest (with S9) Genotoxicity Scores. The scores from Table 3 were plotted against concentration level. Concentrations were independent of volume of sample added into each well (20 μL, 10 μL, and 5 μL). Concentrations (in w/w) are consistent with those in Table 1. Approximate dose responsive curve was attained for test samples when compared to positive control (2AA).

Sodium nitrite reached a maximum genotoxicity score of 4 at a concentration between 0.375% and 0.750% at a volume of 5 μL after metabolic activation. The genotoxicity trend was fairly constant across the three testing volumes; concentrations between 0.188% and 0.750% were most genotoxic, and concentrations above or below this range had lower levels of genotoxicity (**Figure 4**). Metabolic activation increased genotoxicity, confirming the expected outcome.

Potassium sulfate induced low levels of genotoxicity, and metabolic activation did not have an effect on the results. None of the wells displayed acute toxicity and all had some level of color development. The maximum genotoxicity score was 2, which was obtained as concentrations approached a range of 0.063% to 0.250% (**Table 2**). Genotoxicity levels continued to be the highest at this concentration range after

the inclusion of the S9 fraction as well (**Table 3**).

Hydrogen peroxide caused acute toxicity except at a 0.047% concentration at a volume of 5 μL, which reached a genotoxicity score of 3 (**Table 2**). After metabolic activation, all wells had some level of color development signifying metabolic effects on the level of genotoxicity. At a 3.000% concentration, a genotoxicity score of 5 was obtained, and genotoxic activity decreased as the concentration decreased (**Table 3**). A dose responsive curve was obtained for hydrogen peroxide (**Figure 4**). This trend was observed for all three volumes tested.

We hypothesized that the sodium nitrite would be the most genotoxic because nitrites are precursors to *N*-nitrosamines. We predicted that after metabolic activation, the genotoxicity of sodium nitrite would increase as nitrosation can occur during metabolism (10). We hypothesized that potassium sulfate would be genotoxic because sulfates can affect the mitotic index of cells, which can lead to proliferation, and hydrogen peroxide was hypothesized to be genotoxic because it creates free radicals that induce oxidative stress (17, 12). Potassium sulfate and hydrogen peroxide were not predicted to have differing levels of genotoxicity after metabolic activation as they are byproducts of metabolism (12). These hypotheses were partially supported by the outcomes of this project.

DISCUSSION

Our hypotheses were partially supported by our data, as the synthetic food preservatives were genotoxic and caused DNA damage to the *E. coli*. Clear qualitative analysis reveals that *de novo* synthesis of β-gal and subsequent degradation of X-gal occurred as a result of the triggering of the SOS response. Synthetic food preservatives were indeed genotoxic and caused DNA damage to the *E. coli*. Sodium nitrite and hydrogen peroxide were affected by the addition of the S9 fraction as well. Genotoxicity levels of sodium nitrite significantly increased after metabolic activation, and the bacteria were able to survive after hydrogen peroxide was metabolized. Potassium sulfate activity was not impacted by S9 supplementation as initially predicted.

While the underlying mechanism behind the genotoxicity of the food preservatives is unknown, previously conducted research suggests several potential mechanisms. Sodium nitrite may be genotoxic because nitrites are precursors to NOCs. Research shows that NOC production is related to an increase in cancer because NOCs have the capability to inactivate tumor suppressor genes (3). Many of the enzymes used in nitrosation, which leads to NOC formation, are also used in metabolism. This may explain why the genotoxicity increased with the inclusion of the S9 fraction (16).

Potassium sulfate may have been genotoxic because sulfates can cause DNA damage by inactivating genes that regulate cell proliferation. They also affect cell signaling pathways that play a role in controlling cell division and synthesis of new DNA (11). This is one of the most common forms of DNA damage and can possibly explain why the

potassium sulfate displayed genotoxicity under both testing conditions (+/- S9).

Hydrogen peroxide may be leading to acute toxicity because the concentrations and testing volumes were too high. At the lowest concentration and lowest testing volume however, hydrogen peroxide was genotoxic. This may account for the genotoxicity increasing at lower concentrations, but it may also be indicative of a false positive. Hydrogen peroxide was metabolized in the second experiment and although it did not kill the bacteria, it displayed genotoxicity. This suggests the S9 fraction contained enzymes that break apart hydrogen peroxide into components that are genotoxic (16). As in previous studies, hydrogen peroxide most likely caused damage to the DNA through oxidative stress due to its ability to remove electrons from nitrogenous bases (12).

By including the S9 fraction, the results display that the test samples were genotoxic after interacting with enzymes found in mammalian metabolism. Further research would elucidate the underlying mechanisms behind the demonstrated genotoxic effects. It may also lead to potential cures and preventative measures against DNA damage and tumorigenesis linked with certain food preservatives. If no actions are taken, the general well-being of the population may continue to be at risk from DNA damage created by the extensive consumption of synthetic food preservatives (18).

Sterility, negative, and positive controls were performed in both experiments because of the variability in reaction of the *E. coli* and reagents; each plate required independent sets of controls. The variability of each individual SOS Chromotest due to high sensitivity explains why identical concentrations generated differing results (15). By repeating the controls, comparable baseline data were obtained for each individual experiment. Experimental error includes the possibility of contamination of the equipment or bacterial contamination, which we attempted to avoid by using aseptic techniques and an autoclave. Another area of concern was the viability of the bacteria. As a precautionary measure, *E. coli* were transformed to carry ampicillin resistance and were further selected with ampicillin. The negative control also served to reveal the viability of the bacterial cells (18). The negative and sterility controls in the second plate served to show the S9 fraction was not capable of cleaving β-gal or affecting the reagents and therefore inducing a color change. Some samples created an inverse dose responsive curve in which genotoxicity increased as concentration decreased. This may be attributed to experimental error or may have occurred because at higher concentrations, greater levels of repair in the bacteria were activated, reducing the subsequent color change (15).

Various steps can be taken to improve the understanding in this field of research. Different types of assays that determine genotoxic potential should be performed. The experiments performed in this project should be repeated using the Ames test, which uses *Salmonella* to determine if chemical compounds are genotoxic and have caused mutations. The Ames assay would be beneficial to supporting our conclusions, as it can reveal whether our results extend to other organisms, and can give a measure of colony-forming units to understand the decreased bacterial viability caused by hydrogen peroxide in greater detail (15). The comet assay is another technique that determines the level of DNA damage incurred by a cell by measuring strand breaks in DNA. It can display the type of DNA damage caused by synthetic food preservatives by offering a broad view of the extent of DNA damage (14). By using different assays, the accuracy of the method used in our project can be evaluated, and our results can be validated.

In conclusion, this study provides valuable insight into the genotoxicity of commonly used synthetic food preservatives. Further evaluation on food extracts can serve as a more representative model of how much of these food preservatives are truly being consumed. Additionally, further work in the field can lead to increased awareness by the population and Food and Drug Administration and open up avenues for alternative methods of food preservation to lead to a healthier lifestyle globally.

MATERIALS AND METHODS
Bacterial strain
The bacterial strain used in this study was PQ37, derived from *E. coli* through several mutations including the fusion of the LacZ gene with the S*fi*A promoter. The cell membrane was also made more permeable to allow easier flow of test samples. The bacteria was sourced from Environmental Bio-Detection Products (EBPI).

Preparation of S9
4% v/v concentration S9 solution was prepared (16) by mixing liquid rat liver extract with the following cofactors: 8 mM $MgCl_2$, 33 mM KCl, 100 mM sodium phosphate buffer pH 7.4, 5 mM glucose-6-phosphate, and 4 mM NADP. Rat liver extract and cofactors were obtained from EBPI.

Design and procedure for SOS Chromotest with and without S9 fraction
All reagents and materials were purchased from Environmental Bio-Detection Products (EBPI). 3% w/w concentration sodium nitrite solution and a 1% w/w concentration potassium sulfate solution were prepared using double distilled water. The *E. coli* was hydrated with 10 mL of growth medium and 32 µg/mL ampicillin and placed in a shaking incubator at 37º C for 16 hours to reach logarithmic growth. Using a spectrophotometer (Fisher Scientific), the optical density of the bacteria at 600 nm was checked and diluted to 0.05 absorbance with fresh growth medium. 96-well plates were prepared in a setting in which column 1 contained the negative control, column 2 contained the positive control (4NQO), column 3 contained the S9 positive control (2AA), and columns 4-12 contained the test sample columns (**Table 1**). Each food preservative had three columns

and three different testing volumes (20 µL, 10 µL, and 5 µL). Reagents were pipetted into the wells using aseptic techniques. DMSO-saline was pipetted into respective wells to be used as a bacterial solvent. Two-fold serial dilutions were performed for the positive controls and repeated for all three food preservatives. 100 µL of bacterial suspension was added to all wells except the sterility control group (row H). The second plate contained the bacterial suspension, as well as 100 µL of the prepared S9 mix. Once the plates were completely prepared, they were incubated for 2 hours at 37° C. 50 µg/mL X-gal was pipetted into each well and the plates were incubated for an additional hour at 37° C. Blue color development was analyzed and number values were assigned based on blue intensity as compared to the positive, negative, and sterility controls.

REFERENCES

1. Gould, Grahame W. "Methods for Preservation and Extension of Shelf Life." *International Journal of Food Microbiology*, vol. 33, no. 1, Nov. 1996, pp. 51–64., doi:10.1016/0168-1605(96)01133-6.
2. Gömürgen, Ayşe Nihal. "Cytological Effect of the Potassium Metabisulphite and Potassium Nitrate Food Preservative on Root Tips of Allium Cepa L." *Cytologia*, vol. 70, no. 2, June 2005, pp. 119–128., doi:10.1508/cytologia.70.119.
3. Mirvish, Sidney S., et al. "Total N-Nitroso Compounds and Their Precursors in Hot Dogs and in the Gastrointestinal Tract and Feces of Rats and Mice: Possible Etiologic Agents for Colon Cancer." *The Journal of Nutrition*, vol. 132, no. 11, 1 Nov. 2002, doi:10.1093/jn/132.11.3526s.
4. Mersch-Sundermann, V., et al. "The Genotoxicity of Unsubstituted and Nitrated Polycyclic Aromatic Hydrocarbons." *Anticancer Research*, vol. 13, no. 6A, Oct. 1993, pp. 2037–2048.
5. Phillips, David H., and Volker M. Arlt. "Genotoxicity: Damage to DNA and Its Consequences." *Experientia Supplementum Molecular, Clinical and Environmental Toxicology*, 2009, pp. 87–110., doi:10.1007/978-3-7643-8336-7_4.
6. De Bont, R. "Endogenous DNA Damage in Humans: a Review of Quantitative Data." *Mutagenesis*, vol. 19, no. 3, May 2004, pp. 169–185., doi:10.1093/mutage/geh025.
7. O'Connor, C. M. & Adams, J. U. *Essentials of Cell Biology*. Cambridge, MA: NPG Education, 2010.
8. Fernández-Medarde, A., and Eugenio Santos. "Ras in cancer and developmental diseases." *Genes Cancer*. 2011; 2(3):344-58.
9. Dubrow, R., et al. "Dietary Components Related to N-Nitroso Compound Formation: A Prospective Study of Adult Glioma." *Cancer Epidemiology Biomarkers & Prevention*, vol. 19, no. 7, July 2010, pp. 1709–1722., doi:10.1158/1055-9965.epi-10-0225.
10. Song, Peng, et al. "Dietary Nitrates, Nitrites, and Nitrosamines Intake and the Risk of Gastric Cancer: A Meta-Analysis." *Nutrients*, vol. 7, no. 12, 1 Dec. 2015, pp. 9872–9895., doi:10.3390/nu7125505.
11. Vally, Hassan, and Neil L. A. Misso. "Adverse reactions to the sulphite additives." *Gastroenterology and Hepatology from Bed to Bench*, vol. 5, no. 1, Winter 2012, pp. 16-23.
12. Benhusein, Ghazallam., et al. "Genotoxic Effect Induced by Hydrogen Peroxide in Human Hepatoma Cells Using Comet Assay." *Libyan Journal of Medicine*, vol. 5, no. 1, 13 Jan. 2010, p. 4637., doi:10.3402/ljm.v5i0.4637.
13. Jackson, Stephen P., and Jiri Bartek. "The DNA-Damage Response in Human Biology and Disease." *Nature*, vol. 461, no. 7267, 22 Oct. 2009, pp. 1071–1078., doi:10.1038/nature08467.
14. Janion, Celina. "Inducible SOS Response System of DNA Repair and Mutagenesis in Escherichia Coli." *International Journal of Biological Sciences*, 23 Sept. 2008, pp. 338–344., doi:10.7150/ijbs.4.338.
15. Quillardet, P., et al. "SOS Chromotest, a Direct Assay of Induction of an SOS Function in Escherichia Coli K-12 to Measure Genotoxicity." *Proceedings of the National Academy of Sciences*, vol. 79, no. 19, Oct. 1982, pp. 5971–5975., doi:10.1073/pnas.79.19.5971.
16. Registre, Marilyn, and Ray Proudlock. "The In Vitro Chromosome Aberration Test." *Genetic Toxicology Testing*, 2016, pp. 207–267., doi:10.1016/b978-0-12-800764-8.00007-0.
17. Nair, B., and A. R. Elmore. "Final Report on the Safety Assessment of Sodium Sulfite, Potassium Sulfite, Ammonium Sulfite, Sodium Bisulfite, Ammonium Bisulfite, Sodium Metabisulfite and Potassium Metabisulfite." *International Journal of Toxicology*, vol. 22, no. 2 Suppl, 2003, pp. 63–88., doi:10.1080/10915810305077x.
18. Clancy, Suzanne. "DNA damage & repair: mechanisms for maintaining DNA integrity." *Nature Education*, vol. 1, no. 1, 2008, pp. 103.

Article

Characterizing quorum sensing-induced bioluminescence in variable volumes with *Vibrio fischeri* using computer processing methods

Maryam G. Abdel-Azim[1] and Gamal A. Abdel-Azim[2]
[1]Classical Charter School, Appleton, Wisconsin
[2]URUS Group, Research & Development, Madison, Wisconsin

SUMMARY

Bacteria use the mechanism of quorum sensing to gather information about the density of other cells in their surroundings. Quorum sensing, in which bacteria sense chemical signals that increase in concentration as a function of surrounding cell density, leads to downstream changes in bacterial gene expression. These changes may include the activation of virulence or bioluminescence. In this study, we used *Vibrio fischeri* as a model to study the activation of bioluminescence by quorum sensing. We inoculated the same number of bacterial cells in 3 different culture volumes (1mL or small volume, 3mL or medium volume, and 5mL or large volume) and measured luminescence of the cultures over time. Using digital image processing to determine changes in luminescence over time, we found that cultures in smaller volumes reached peak illumination densities in less time than those in larger volumes. These results suggest that *V. fischeri* luminesce in response to cell density information in the environment and that we can use computer processing methods to study quorum sensing-induced bioluminescence. Studying the mechanisms by which bacteria use quorum sensing to activate gene expression may facilitate the development of therapies to inhibit bacterial virulence in the context of infectious disease.

INTRODUCTION

Cell-to-cell communication that is used to share information about bacterial cell density in the surrounding environment is called quorum sensing (1). Bacterial cells release autoinducers, which are chemical signaling molecules that other bacterial cells sense and use to collect information about cell density in the environment. Based on the acquired cell density information, bacteria behave collectively in a synchronous manner to regulate gene expression, which results in the activation of specific traits such as virulence or bioluminescence. Physiological activities that are regulated by quorum sensing include symbiosis, virulence, competence, conjugation, antibiotic production, motility, sporulation, and biofilm formation (2).

Vibrio fischeri is a Gram-negative marine organism that was initially used to investigate quorum sensing (3). When population density reaches a certain threshold *V. fischeri* activate bioluminescence through a concerted response process (4). In the quorum sensing cycle of *V. fischeri* (**Figure 1**) the main responsible genes are luxR and luxI (5). The luxI
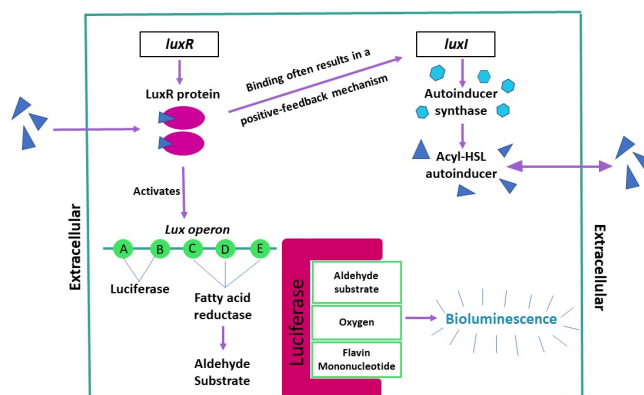

Figure 1. A schematic of the quorum sensing cycle in *V. fischeri*.

gene codes for an autoinducer synthase that synthesizes the acyl-HSL autoinducer (6). The luxR gene encodes for a LuxR protein that recognizes autoinducers released into the environment by other bacterial cells (5, 7). The lux operon is an inducible operon that is comprised of genes that are responsible for bioluminescence. Once the autoinducer is bound to the LuxR protein, the complex activates the lux operon, luxCDABE (6, 8). luxA and luxB encode for subunits of luciferase, which catalyzes the bioluminescence reaction (5). luxCDE encode for a fatty acid reductase, which synthesizes the aldehyde substrate. The luciferase enzyme is used to catalyze the reaction of the aldehyde substrate, diatomic oxygen, and flavin mononucleotide to trigger bioluminescence (9). The binding process of the autoinducers and luxR results in a positive-feedback mechanism that further increases the concentration by inducing the transcription of the cognate luxI signal synthase gene (8).

The activation of the bioluminescence in *V. fischeri* is especially important to the bobtail squid, a nocturnal creature that uses the light emitted from the bacteria to hide from predators. Studies have also shown that quorum sensing can be triggered in other species of bacteria even for a single cell confined in a micro droplet as a result of the accumulation of signaling molecules produced by the confined cell (10).

Quorum sensing depends on cell density, defined as the total number of cells per milliliter. We hypothesized that quorum sensing is triggered much faster when bacteria is cultured in smaller volumes than when cultured in larger volumes of media. In this study we validated this hypothesis by first showing that quorum sensing can be activated at
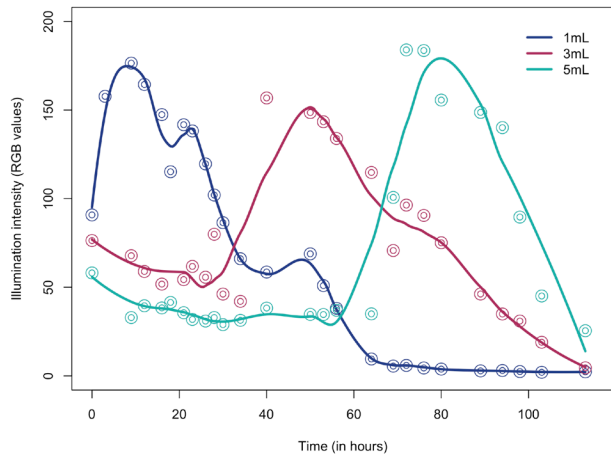
Figure 2. Progression of the 1mL, 3mL, and 5mL cultures toward maximum illumination. After peaking at maximum RGB intensity, bioluminescence gradually declined toward an RGB value of 0. Each point represents the mean illumination intensity of multiple images taken at the same time. The curve was developed by the 'loess' function in R which locally fitted illumination data against time in hours.
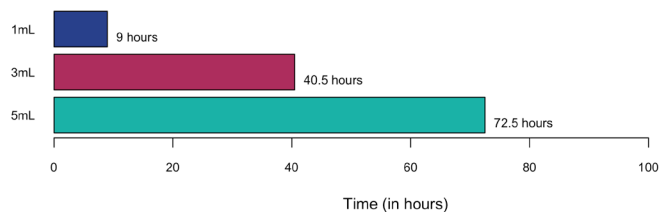

Figure 3. Bar plot of the time that each volume took to reach maximum illumination. Greater volumes took significantly more time to reach their peak intensity than smaller volumes.

quorum sensing using computer processing of high-quality digital images. Finally, we characterized the variation in the quorum sensing lifecycle of *V. fischeri* in small, medium, and large volumes. We showed that, with the same starting number of cultured cells, higher densities of cells were attained more quickly in smaller culture volumes than in larger culture volumes. This study proved the dependency of quorum sensing on cell density by using computer processing techniques on captured digital images.

RESULTS

To investigate the effect of quorum sensing in *V. fischeri*, cultured in variable volumes, we inoculated the same number of bacterial cells in 3 different culture volumes (1mL or small volume, 3mL or medium volume, and 5mL or large volume) and measured luminescence of the cultures over time. RGB color values were utilized to characterize illumination levels of digital images taken for *V. fischeri* cultures. Values were averaged for all pixels of an image and were shown to precisely evaluate illumination levels across images.

Volume (mL)	Average illumination (RGB intensities)		Time to peak illumination (hours)
	At starting time	At peak time	
1	90.8	176.5	9.0
3	76.4	156.8	40.5
5	58.1	183.9	72.5

Table 1. Average illumination at starting and peak time for all three volumes expressed as RGB pixel intensities. Time intervals in hours from starting to peak time are shown.

Volume (mL)	Avg. final illumination (RGB intensities)	Time from peak to loss of illumination (hours)
1	4.5	67.5
3	4.5	73.0
5	25.5	41.0

Table 2. Average illumination at final time for all three volumes expressed as RGB pixel intensities. Time intervals in hours from peak to loss of illumination are shown.

Time (hrs.)	Trend	Slope	Std Error	*P* Value
1mL				
0 - 9	Upward	8.603	1.371	< 0.001
9 - 69	Downward	-2.609	0.091	< 0.001
3mL				
30 - 40	Upward	11.702	1.393	< 0.001
> 40	Downward	-2.335	0.103	< 0.001
5mL				
64 - 72	Upward	18.306	3.913	< 0.001
> 72	Downward	-4.418	0.341	< 0.001

Table 3. Slope estimates of illumination intensity on time in hours. Slopes were estimated for volumes 1, 3 and 5 mL from the time of quorum sensing activation to peak illumination and from the time of peak illumination to loss of illumination.

Full quorum sensing cycles of cell culture volumes of 1, 3, and 5 mL are shown in **Figure 2**. Because higher cell densities were attained earlier in smaller volumes, the starting and peaking times for quorum sensing were different for the three volumes studied. In smaller volumes, quorum sensing was activated and peaked at a faster rate than in larger volumes. The average times to reach peak illumination were 9, 40.5, and 72.5 hours for volumes 1, 3, and 5 mL, respectively (**Figure 3**). The RGB values of the volumes were low at starting time and reached their highest at peak time (**Table 1**). To characterize illumination after its peak for each of the three volumes, the average time between peak and loss of illumination and average RGB values at final illumination were calculated. Final illumination of the 5 mL volume averaged higher than other volumes because of its shorter time span between peak and final illumination (**Table 2**).

We studied the rate of illumination progress toward the peak versus the rate of illumination decline after the peak. The rate of the progress toward the peak was higher than the rate of decline after the peak in all volumes (**Figure 2**). We estimated slopes of illumination intensity over time for volumes 1, 3 and 5 mL during the intervals from the activation of quorum sensing to peak illumination (upward trend) and from the time of peak illumination to total loss of illumination (downward trend). These slope estimates showed that the
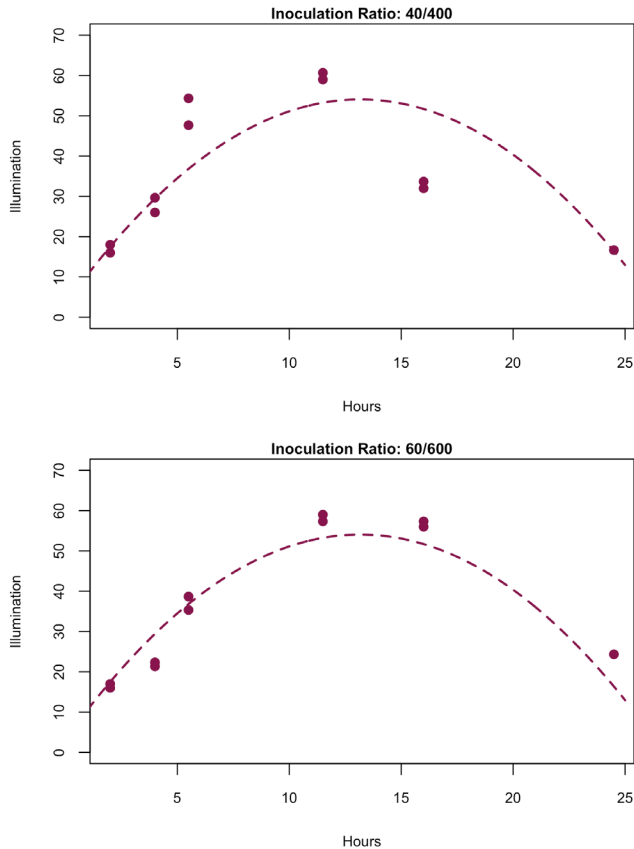
Figure 4. Plot of pixel intensities of each of 2 images taken at each time for the 2 sets of vials with proportional inoculation. Curves shown modeled the quadratic trend of quorum sensing using a 2nd degree equation estimated from data. Maximum illumination occurred at the same time (11.5 hours) in the two volumes because of their equal starting cell densities.
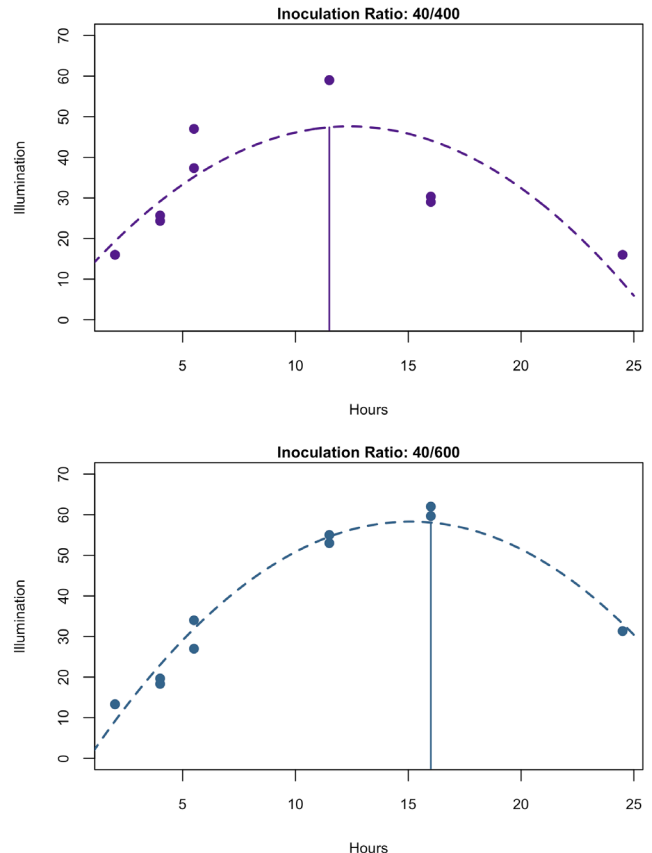
Figure 5. Plot of pixel intensities of each of 2 images taken at each time for the 2 sets of vials with fixed inoculation amount in small and large volumes of media. Curves shown modeled the quadratic trend of quorum sensing using a 2nd degree equation estimated from data. Maximum illumination occurred 4.5 hours earlier in the small than in the larger volume of media.

rate in the upward trend was 3 to 5 times greater than the absolute rate in the downward trend. *P* values were less than 0.001, indicating that slope estimates were significantly different from 0 (**Table 3**).

As explained earlier (**Figure 1**), the binding process of the acyl-HSL autoinducers and LuxR results in a positive-feedback mechanism that further increases the concentration of autoinducers. Results in **Table 3** of the slopes agreed with the positive feed-back mechanism which causes quorum sensing to accelerate at a higher rate toward peak illumination.

As expected, when the starting cell densities in small and large volumes of media were the same due to proportional inoculation, quorum sensing was triggered simultaneously. However, when the starting cell densities were different due to fixed inoculation in variable volumes, quorum sensing was triggered earlier in the media with greater starting cell density (**Figure 4**). Maximum illumination occurred after 11.5 hours in both volumes because of the equal starting cell densities (**Figure 4**). On the other hand, an earlier illumination could be found for the smaller volume after 11.5 hours versus 16 hours for the greater volume (**Figure 5**). The smaller volume peaked earlier as a result of its higher starting cell densities.

Based on these results, we chose to keep the starting

amount of culture constant, while varying volumes. Throughout the study smaller volumes implied higher starting cell densities, with the hypothesis of reaching the required threshold for quorum sensing earlier than larger volumes.

DISCUSSION

By varying volumes of growth media while keeping the amount of the starting culture fixed, we demonstrated that quorum sensing was triggered earlier in smaller volumes when compared to larger volumes. *V. fischeri* cultures in smaller volumes reached their maximum illumination intensity in shorter periods of time than in larger volumes, as a result of the higher starting cell density and the faster progress toward the density threshold required to trigger quorum sensing. Moreover, in all volumes, upward trends toward peak illumination were found to display an accelerated rate when compared against downward trends, which was a common feature in quorum sensing cycles of all volumes studied. This could have been the result of the positive-feedback mechanism, however, there could be other explanations for these results, for example, the bioluminescence state might be very stable once it is triggered, and it requires more time before it turns off.
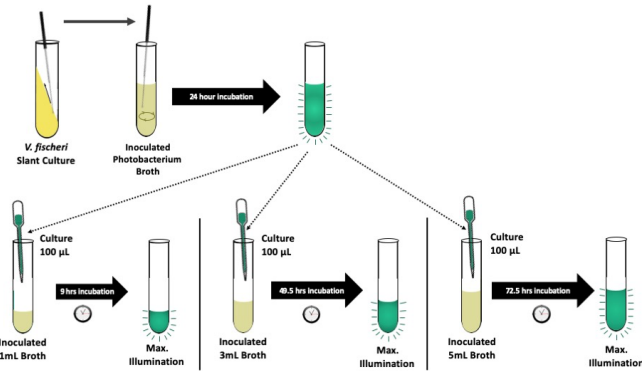
Figure 6. Experimental design. First, *V. fischeri* slant culture was used to prepare a stock of bacteria. Second, 3 different volumes of photobacterium broth were inoculated from the stock and incubated for 80 hours.

Figure 7. An example cropped image displayed to show how its pixel intensities were calculated and analyzed in R.

In this study, we developed a method to characterize quorum sensing in *V. fischeri* using RGB illumination intensity values of pixels in digital images. The RGB approach was shown to be precise in quantifying illumination based only on a high-resolution camera and image processing software. While it is common to use a luminometer to measure bacterial bioluminescence (e.g., 11), we introduce a simpler and more informative approach of gathering illumination data from digital images.

Studying the mechanisms by which bacteria use quorum sensing to activate gene expression may facilitate the development of therapies to inhibit virulence in bacterial strains in the setting of infectious disease.

Although *V. fischeri* is not disease-causing bacteria, it serves as an experimental model for studying and controlling quorum sensing. Methods to deactivate quorum sensing in *V. fischeri* can be tested while illumination levels are more efficiently tracked using image processing approaches introduced here. This makes it easier to then transfer quorum sensing inhibitors studied to disease-causing strains of bacteria at a later research phase (12, 13).

MATERIALS AND METHODS

Broth Preparation

Gram-negative *V. fischeri* and dehydrated photobacterium broth were purchased from Carolina Biological Supply Company. To prepare the photobacterium broth, 15.2 mL of distilled water were added to every gram of dehydrated photobacterium broth. The broth was mixed thoroughly to ensure that all of the solute was dissolved to achieve a hydrated photobacterium broth with a concentration of 65.8 mg/mL. The prepared broth was then sterilized by placing it into a pressure autoclave for 50 minutes.

Culture Preparation

Living *V. fischeri* bacteria cultured on photobacterium agar at 25°C in a tube were obtained from Carolina Biological Supply Company. Sterilized broth was then pipetted in test tubes which were inoculated with the living *V. fischeri* bacteria using a sterilized inoculating loop. The test tubes were incubated at 25°C for 24 hours on an orbital shaker with 200 rotations per minute. The purpose was to prepare liquid bacterial cultures to use in subsequent experimental steps, which required precise concentrations of bacterial cultures to inoculate broth in tubes with variable volumes.

Experimental design

One objective of the current study was to use variable volumes to validate the dependency of quorum sensing on cell density. In a smaller volume, less time is needed for autoinducers to reach the threshold required for bioluminescence, while in a larger volume, more time is needed for autoinducers to reach the same threshold. Volumes 1, 3, and 5 mL were chosen throughout the experiment to represent small, medium, and large culture volumes. Smaller culture volumes were expected to reach the autoinducer density threshold of bioluminescence faster than larger volumes, as volume and density are indirectly related, where cell density = total number of cells/volume.

To measure time to bioluminescence per volume, 2 test tubes per volume were prepared for a total of 6 tubes of sterile photobacterium broth. Each of the six test tubes was inoculated with 100 µL of the liquid bacterial culture prepared earlier (**Figure 6**). All test tubes were incubated in a dark chamber with no external light source at 25°C on an orbital shaker set to 200 rpm. At the end of each experiment, live cultures were disposed of properly after bleaching all test tubes.

Acquisition of digital images

High resolution images were taken using a Canon EOS Rebel T6 camera with a 30-second exposure at ISO 3200. All images were taken with no zoom using the same settings and placement for both the camera and test tubes. High resolution still digital images were taken for the bacteria in triplicate in a completely dark chamber every 1-2 hours to monitor the progression of bioluminescence levels for a total of 80 hours. The 80-hours monitoring period was the time necessary for all three volumes to go through the full bioluminescence cycle
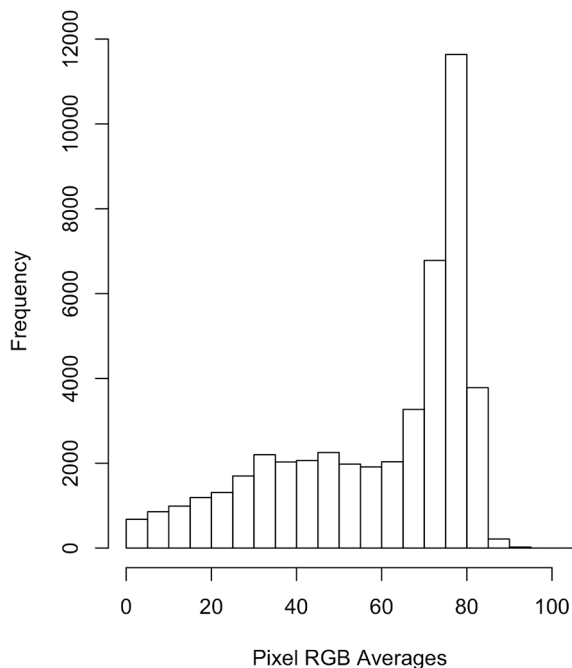
Figure 8. Bar plot of pixel intensities of an example image. The bar plot shows a high frequency for pixels with intensities ranging from 65 to 85 in their average RGB values.
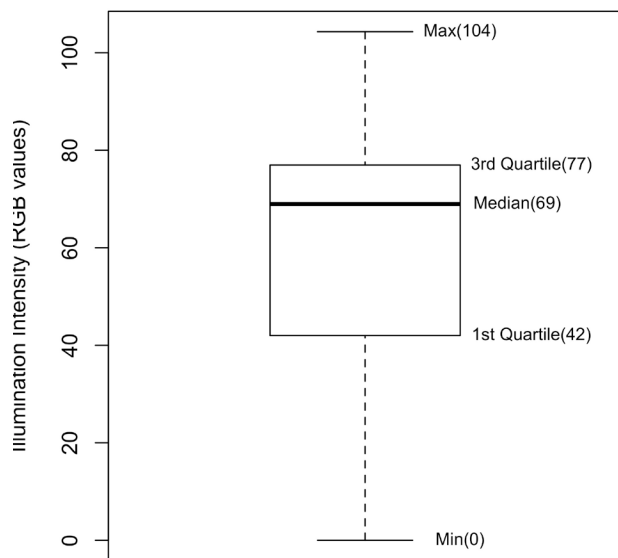

Figure 9. Box plot of pixel intensities of an example image. The box plot shows RGB range of values from 0 (completely dark) to a maximum of 104 (fairly luminescent). Summary statistics are also labeled on the box plot.

of reaching peak illumination and gradually dimming down to zero light emission.

Detection and measurement of illumination intensity in digital images

Images were converted into quantities amenable for statistical analysis by averaging the R, G, and B values of each pixel (**Figure 7**). The R, G, and B values of each pixel in the image were averaged to quantify pixel intensities. To
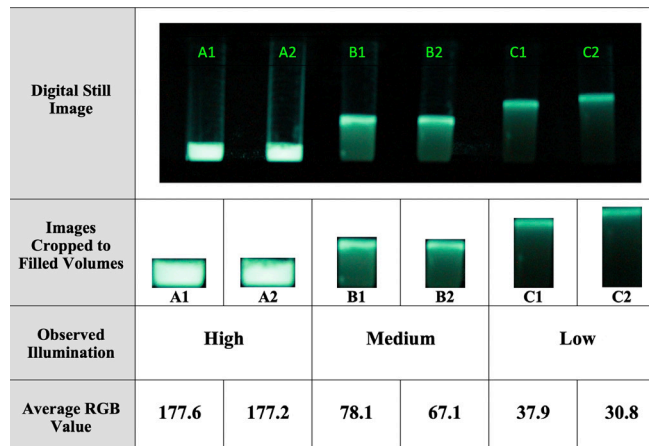

Figure 10. Test tubes with *V. fischeri* illuminating at different intensities. Corresponding average pixel RGB values of the filled volumes are shown.

study image illumination further, a histogram of pixel intensities was created (**Figure 8**). The histogram shows pixel intensities, ranging from 65 to 85, to be of the highest frequency in the image. Finally, a boxplot of pixel intensities was developed and labeled to show the summary statistics of pixel intensities in the image (**Figure 9**). The boxplot shows the minimum and maximum values as well as the mean and the median; it also displays the 1st and 3rd quartiles of pixel intensities in the image. The R code used to read images and transform them into RGB data is available online (14).

Digital still images were taken for test tubes with *V. fischeri* grown in photobacterium medium while illuminating. Images of 6 test tubes at specific illumination levels were taken. The objective was to interpret colors in images taken into meaningful values to differentiate between high and low illumination intensities. To achieve this objective, the RGB color values of each pixel in the images were measured as shown above. The RGB color values quantify the combination of Red, Green, and Blue colors, where their average associates directly with the intensity of light emitting from each pixel in the image. The average was preferred to the median because of its sensitivity towards extremely low- or high-illumination pixels.

The average RGB values of tubes A1 and A2 were near 177, of tubes B1 and B2 were 67 to 78, and of tubes C1 and C2 were 31 to 38 (**Figure 10**). Average pixel RGB values of the filled volumes in the tubes were shown to correctly identify the level of illumination intensity observed. Therefore, average pixel RGB values were used throughout this experiment as a measure for light emission.

Proportional versus fixed starting culture

To decide between using fixed or proportional inoculum, a short study was performed to validate the hypothesis that smaller volumes reach higher cell densities faster than larger volumes when the amount of the starting culture is the same. The impact of proportional versus fixed starting

culture volumes was compared in two pilot trials. In the first trial, 40 and 60 μL of starting culture were used to inoculate 400 and 600 μL of sterile media in vials, respectively. This proportional inoculation was performed to have the same starting cell densities in small and large volumes of media. In the second, a fixed amount of 40 μL of starting culture was used to inoculate another set of 400 and 600 μL of sterile media. The fixed-volume inoculum in two different volumes was performed to have variable starting cell densities. Two vials of each combination of inoculum and media volumes were used with images taken over a period of 24 hours.

REFERENCES

1. Rutherford, Steven T., and Bonnie L. Bassler. "Bacterial Quorum Sensing: Its Role in Virulence and Possibilities for its Control". *Cold Spring Harbor Perspectives in Medicine*, vol. 2, no. 11, 2012, doi:10.1101/cshperspect.a012427.

2. Miller, M. B., and B. L. Bassler. "Quorum Sensing in Bacteria". *Annual Review of Microbiology*, vol. 55, 2001, pp. 165-199, doi:10.1146/annurev.micro.55.1.165.

3. Kempner, E. S., and F. E. Hanson. "Aspects of Light Production by Photobacterium Fischeri". *Journal of Bacteriology*, vol. 95, no. 3, 1968, pp. 975-979.

4. Kleerebezem, Michiel. "Quorum Sensing Control of Lantibiotic Production; Nisin and Subtilin Autoregulate their Own Biosynthesis." Peptides, vol. 25, no. 9, 2004, pp. 1405-1414, doi:10.1016/j.peptides.2003.10.021.

5. de Kievit, T. R., and B. H. Iglewski. "Bacterial Quorum Sensing in Pathogenic Relationships". *Infection and Immunity*, vol. 68, no. 9, 2000, pp. 4839-4849, doi:10.1128/iai.68.9.4839-4849.2000.

6. Fuqua, C., S. C. Winans, and E. P. Greenberg. "Census and Consensus in Bacterial Ecosystems: The LuxR-LuxI Family of Quorum-Sensing Transcriptional Regulators". *Annual Review of Microbiology*, vol. 50, 1996, pp. 727-751, doi:10.1146/annurev.micro.50.1.727.

7. Bassler, B. L. "How Bacteria Talk to each Other: Regulation of Gene Expression by Quorum Sensing". *Current Opinion in Microbiology*, vol. 2, no. 6, 1999, pp. 582-587, doi:10.1016/s1369-5274(99)00025-9.

8. Abisado, Rhea G., et al. "Bacterial Quorum Sensing and Microbial Community Interactions." *MBio*, vol. 9, no. 3, 2018, doi:10.1128/mbio.02331-17.

9. Stevens, A. M., and E. P. Greenberg. "Quorum Sensing in Vibrio Fischeri: Essential Elements for Activation of the Luminescence Genes." *Journal of Bacteriology*, vol. 179, no. 2, 1997, pp. 557-562, doi:10.1128/jb.179.2.557-562.1997.

10. Boedicker, James Q., Meghan E. Vincent, and Rustem F. Ismagilov. "Microfluidic Confinement of Single Cells of Bacteria in Small Volumes Initiates High-Density Behavior of Quorum Sensing and Growth and Reveals its Variability". *Angewandte Chemie (International Ed. in English)*, vol. 48, no. 32, 2009, pp. 5908-5911, doi:10.1002/anie.200901550.

11. McCann, Jessica, *et al*. "Population Dynamics of Vibrio Fischeri during Infection of Euprymna Scolopes". *Applied and Environmental Microbiology*, vol. 69, no. 10, 2003, pp. 5928-5934, doi:10.1128/aem.69.10.5928-5934.2003.

12. Wang, Rui, *et al*. "Honey's Ability to Counter Bacterial Infections Arises from both Bactericidal Compounds and QS Inhibition". *Frontiers in Microbiology*, vol. 3, 2012, pp. 144, doi:10.3389/fmicb.2012.00144.

13. Singh, Braj R., *et al*. "Scaffold of Selenium Nanovectors and Honey Phytochemicals for Inhibition of Pseudomonas Aeruginosa Quorum Sensing and Biofilm Formation". *Frontiers in Cellular and Infection Microbiology*, vol. 7, 2017, https://www.ncbi.nlm.nih.gov/pmc/articles/PMC5362927/, doi:10.3389/fcimb.2017.00093.

14. Abdel-Azim, Maryam. Luminesce. *GitHub*, 2020. https://github.com/maryamazim/luminesce/blob/master/manu-script.R.

Honey bee pollen in allergic rhinitis healing

Martin Bjelajac[1], Marijana Carić, Ph.D.[2]
[1]E-gimnazija Novi Sad
[2]University Business Academy in Novi Sad, Novi Sad, Serbia.

SUMMARY

The most common atopic disease of the upper respiratory tract is allergic rhinitis. It is defined as a chronic inflammatory condition of nasal mucosa due to the effects of one or more allergens and is usually a long-term problem. Under those conditions, it is desirable to avoid excessive and irrational application of chemical drugs and to consider the use of supplemental medicaments. The purpose of our study was to test the efficiency of apitherapy in allergic rhinitis healing by the application of honey bee pollen. Apitherapy is a branch of alternative medicine that uses honey bee products. Honey bee pollen can act as an allergen and cause new allergy attacks for those who suffer from allergic rhinitis. Conversely, we hoped to prove that smaller ingestion of honey bee pollen on a daily basis would desensitize participants to pollen and thus reduce the severity of allergic rhinitis. We conducted this research with 46 individuals between 22 and 47 years old, treated for allergic rhinitis. The patients filled in a questionnaire, with a visual analogous scale linked with the individual feeling of sneezing and other symptoms of rhinitis before and after the therapy. There was a significant difference (p=0.000; α=0.05) between symptoms of users before and after therapy conducted using honey bee pollen. After the pollen application, we recorded reduced symptoms with all participants and therefore the results support the main hypothesis. According to our research, the application of the honey bee pollen as therapy for allergic rhinitis is efficient and justified. Also, pollen therapy resulted in positive responses with participants suffering from other health issues.

INTRODUCTION

Allergic rhinitis is the most common allergic disease of the upper respiratory tract, affecting 10-30% of the world's population (1). Allergic rhinitis is defined as a symptomatic disorder of the nasal mucosa occurring after contact with allergens in the environment, resulting in an IgE-mediated inflammatory reaction that manifests in several symptoms and signs including nasal congestion, liquid secretion, sneezing, and itching of the nasal mucosa. Therefore, allergic rhinitis is a type I hypersensitivity, or anaphylactic reaction. After contact of the respiratory mucosa with inhaled allergens (pollen of trees, grasses, and weeds, household dust, mites, feathers, animal hair, mold, etc.) in individuals with an atopic constitution, sensitization to allergens will occur. Individuals with atopy are genetically predisposed for excessive, severe reactions to usual allergens that involve abundant production of IgE antibodies (1).

Allergic rhinitis is commonly known as a pollen allergy. The most frequent symptoms include a runny or clogged nose, itchy, teary, or red eyes, as well as sneezing (2). Symptoms that may later, if the condition worsens, include red and inflamed throat, a cough, a clogged nose, and swollen eyelids (3). Although the symptoms are similar to the cold, the difference is that allergens rather than viruses cause rhinitis. Generally, the reaction of an individual's immune system causes allergies; if the immunity is over-reactive the body reacts in the form of allergy when the immune systems come into contact with harmless substances (4). Although it is not a life-threatening disease, allergic rhinitis represents a global health problem because it significantly disturbs the quality of life of patients in a way that seriously reduces focus and workability, and it is often connected with other diseases such as asthma (5).

Without professional consultancy, individuals often take some medicaments, available but not efficient against all types of rhinitis, and do not affect all patients the same way. They often expose themselves to different therapeutic procedures, medically justified or unjustified. The most effective medicaments are nasal sprays or corticosteroids which after long-term application can lead to drying of the nasal mucosa, another issue that can lead to nasal polyposis (6). Using a nasal saline rinse can help to thin and decrease the amount of mucus, although this is not sufficient for healing. In some cases, antihistamines are recommended, but they can result in undesirable reactions such as rash, headache, or sleepiness. In addition to drug therapy, allergic rhinitis can be treated by immunotherapy or allergic vaccination. By injecting increasing concentrations of the patient's allergens, immunotherapy can induce tolerance, which significantly reduces or eliminates the patient's adverse reaction when exposed to the allergens. The down-side of this type of therapy is that it lasts in continuity for at least 3 years (7). Patients who do not react positively to pharmacological therapy and do not wish to take drugs that cause undesirable side-effects opt-in for this therapy (Table 1).

As modern medicine looks for new ideas, apitherapy offers many solutions regarding the fight for global health

Table 1.

Characteristic symptoms of allergic rhinitis
Initial symptoms
o Sneeze onsets, with liquid, and often abundant secretion from the nose
o Hindered breathing through the nose
o Nose itching
o Eyes itching and tears
o Reduced smell ability
Disease complications
o Throat pain
o Paranasal sinuses inflammation
o Ear inflammation
o Asthma
Current treatments for allergic rhinitis
o Antihistamines
o Decongestants
o Intranasal corticosteroids
o Eye drops
o Immunotherapy
o Sublingual immunotherapy (SLIT)

Table 1. Characteristic symptoms of allergic rhinitis. A patient has intermittent allergic rhinitis if symptoms occur less than 4 days a week or 4 weeks of the year. Persistent allergic rhinitis is labeled if symptoms occur more than 4 days per week and more than 4 weeks of the year. Symptoms are classified as mild when the quality of life is not affected. Symptoms are moderate to severe if patients have at least one of the following: sleep disturbance, impairment of daily activities, sports, or leisure, impairment of school or work, or troublesome symptoms (8).

and quality of life. Apitherapy involves the therapeutic use of honey bee products, including bee pollen, honey, propolis, royal jelly, beeswax, and venom, to treat a variety of ailments (9). Modern aspirations in the field of honey bee products are primarily focused on proving their importance in health protection. It can be freely said that the honey bees produce something that neither chemists, pharmacists, technologists nor any other scientist is able to easily create without help from honey bees.

Bees process nectar from the flowers through their organism (specifically honey stomach) and later in a beehive, producing an elixir rich in numerous nutritious and healing ingredients (10). Honey contains organic acids, amino acids, pollen, ether oils, flavonoids, vitamins, minerals, and other valuable components. Sugars produced by the bee honey are most abundant with fructose, followed by glucose and a much smaller fraction of saccharose. Honey contains vitamins B1, B2, B5, B6, C, D, E, and K, and minerals including sodium, potassium, calcium, phosphorus, magnesium, iron, zinc, iodine, copper, chromium, and selenium (11). The most famous healing feature of honey is a reduction of influenza and cold symptoms, as well as other diseases of the respiratory tract such as bronchitis, throat, and sinus inflammation (11). Honey is effective in aiding wound healing because honey works as an antiseptic, while also neutralizing poisons from a bite or sting. Compresses with honey help with and alleviate skin problems such as cracked skin, rash, or itching. Honey is of great help with different digestive problems, such as constipation, gastritis, or ulcers. In addition to its medicinal properties, honey's effect doubles by adding medicinal herbs.

Scientists confirm its antibacterial, antiseptic, and anti-oxidative characteristics (12). Numerous clinical studies have examined the honey effects on cough and they showed it was equally effective as the most often applied citruses (12) (13). Honey bee products (beebread, bee poison, pollen, propolis, and honey) play crucial roles in prophylaxis and treatment of many human diseases. These products contain amino acids, proteins, carbohydrates, balsams, ferments, and microelements for which have been shown to possess antimicrobial, antiviral, antiparasitic, anti-inflammatory, antioxidant, antimutagenic and antitumor effects (14)(15). Recent studies confirmed that enzymes from pollen have an exceptional anti-oxidative effect. Although there is no firm evidence, some studies have suggested that honey bee pollen may even have positive effects in treating cancer, cardiovascular diseases, and diabetes (16).

The honey bee pollen contains almost all healthy nutritive matters necessary for the growth, development, and health of the human organism. In some developed countries, such as Germany and Belgium, it is officially confirmed as a medicament (17). Honey is of greatest quality when honey bees have access to the pollen originating from different herbal species because chemically balanced food is of key importance for a bee colony's development. The greatest influences on the content of certain substances in the pollen are its botanical and geographical origin (18). The pollen varies in its color from light yellow to black. The grains are different shapes, sizes, and weights depending on from where the herbal species the bees collected the powder (19). In stores, bee pollen is available as natural granules. It can also be mixed with other foods like granola, yogurt, or smoothies. Pollen granules generally have a bitter taste, although people with regular intake, adapt to the taste. This diet has to be conducted a few months before the season starts to get any response in the prevention of allergy.

Based on previous studies on honey bee products and the potential to positively affect symptoms of allergic rhinitis, we hypothesized that because pollen comes from plants one may be allergic to, pollen might be able to protect one's immune system from reacting to airborne allergen exposure from those same plants, perhaps by the process of desensitization. Specifically, we hypothesized that gradual intake of increasing concentration of pollen should induce tolerance to allergens by accommodating the organism to newly taken microelements.

RESULTS

The question we explored was whether honey bee pollen helps in the treatment of allergic rhinitis. In order to test this, we conducted research with 46 individuals treated due to allergic rhinitis. Before we began our study, we formed a template with study information. Each participant in our study was provided with a copy of this template, which they reviewed and signed before the study began. We recruited a total of 32 women and 14 men as participants and all

participants were 22-47 years old. The patients filled in the questionnaire before and after the therapy. All participants, within the apitherapy of 45 days, took the pollen produced in the honey bee farmstead (the owner of the farmstead is Mirko Vlahovic, in Crni vrh Berane, entered in the beehive register with the Veterinary Administration of Montenegro by Decision number 060-323113-036-295/2 dated 05/09/2013). The goal of our research was to show that the use of pollen alleviates problems caused by allergic rhinitis.

We divided participants according to the severity of their allergy symptoms (Figure 1). 27 participants had several symptoms that reduced the quality of their life and workability, including sneezing, teary eyes, abundant secretion from the nose, and impeded breathing.

We conducted research in winter, due to fewer allergens present. In spring, when allergies become more severe, we reassessed the change in symptoms to estimate the efficiency of pollen therapy. We instructed participants to maintain a diary and track changes in their symptoms through all 45 days of the therapy, as they gradually increased pollen intake. After therapy ended, we waited 15 more days (where participants continued their diary) into the spring, to analyze the data and see the results. In the spring, participants with seasonal allergies felt that their symptoms were less severe as a result of the treatment. We also noticed a reduction in symptoms in participants who were locals to the place where we collected the pollen for therapies.

Sneezing evaluation and other complications before and after the pollen application showed a statistically significant reduction of symptoms after the therapy ($p < 0.05$). After the therapy, all participants evaluated their complications, and only 1 participant had several symptoms (Figure 2). Pollen therapy had a positive effect on all of the participants. 20 participants did not have any symptoms, 25 participants had to sneeze several times per day, and only 1 participant had sneezing that was frequent but did not disturb daily activities. None of the participants had symptoms that disturbed daily activities.

After we finalized the experiment, the results supported our hypothesis that preventive and controlled intake of honey bee pollen reduces the incidence and severity of allergic rhinitis.

DISCUSSION

According to our research, the application of the honey bee pollen in allergic rhinitis therapy is efficient and justified. Therapy produced a positive response without any undesired effect in participants suffering from other diseases. Our study is in agreement with previous research that supported the efficacy of honey and pollen products in the therapy of pollen allergies with individuals with and without atopic problems or asthma (20).

With the application of pollen and the addition of honey, we recorded notable improvement and ease of complications in the participants who had long-lasting symptoms of rhinitis.
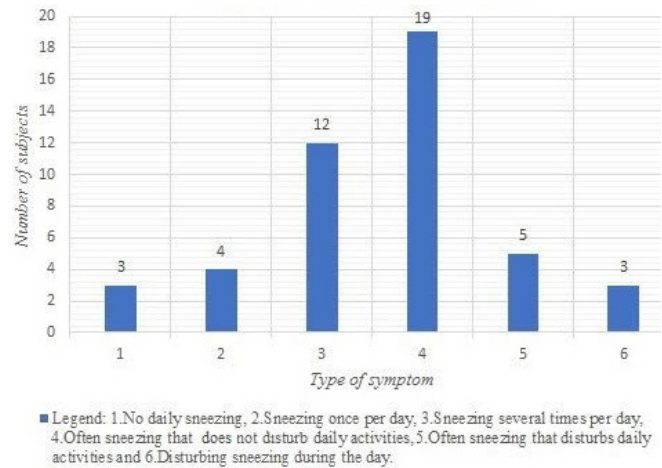

Figure 1. Distribution of participants according to symptoms before the pollen application. Before the application of pollen therapy, the majority of participants (31) experienced a mild symptom of allergic rhinitis: frequent sneezing throughout the day that did not disturb daily activities. Some of our participants (8) experienced a severe symptom of allergic rhinitis: sneezing that disturbs daily activities.
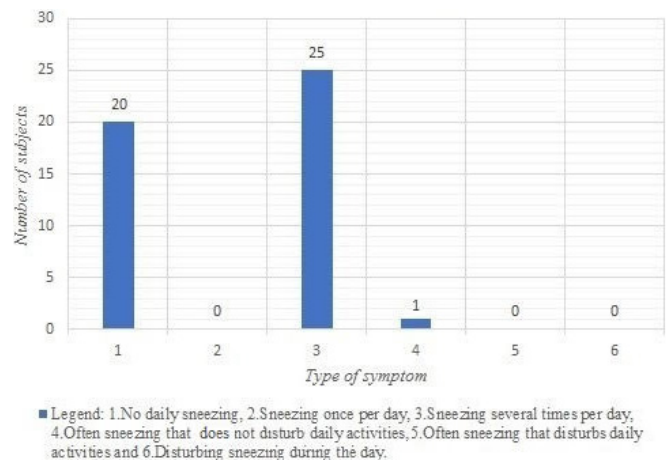

Figure 2. Distribution of participants according to symptoms after the pollen application. After the application of pollen therapy, we notice a significant rise in the number of participants that had no daily sneezing. Some participants still have a mild symptom of allergic rhinitis, but there are no participants with a severe symptom of allergic rhinitis: sneezing that disturbs daily activities.

In our study, participants did not describe undesired effects or allergic reactions, and, as especially important, participants did not report a deterioration of existing problems during the application of the honey bee pollen.

Rhinitis is most commonly a consequence of allergic reactions and it corresponds to the natural flow of the nasal mucosa inflammation. The trend of the use of Over the Counter drugs is increasing. The development of the pharmaceutical industry, through long-term prognosis, shows that honey bee products, as a raw material for medicinal remedies, are of special significance. These products are easily available, therapeutically effective, and possess multisided biologically
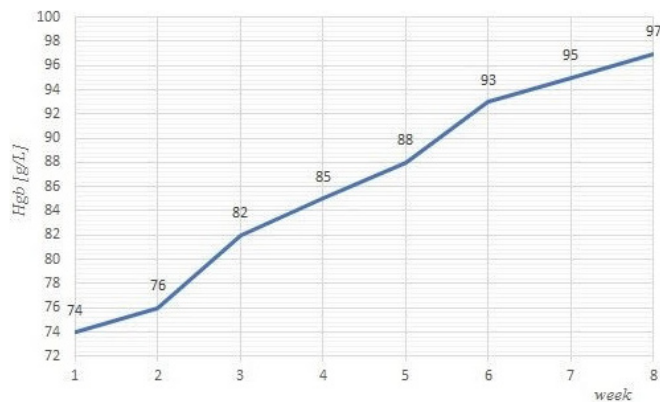
Figure 3. Hemoglobin levels in subject #XX during the course of pollen treatment. Patient #XX was diagnosed with anemia eight years prior to this study. Throughout the course of pollen treatment, this participant underwent weekly blood testing to monitor hemoglobin levels, shown here. A steady increase in hemoglobin levels was observed during this time frame.

active components (21).

Patients suffering from acute and chronic diseases often cannot use antibiotics or antitussive drugs (drugs used to prevent or relieve coughing). Antibiotics have no effect on viral inflammations of the respiratory tract and there is limited evidence for the effectiveness of antibiotics and antitussives on asthma (22). As the specter of the treatment for these problems is reduced, it would be useful to consider apitherapy which, according to studies, reduces cough frequency and severity (23).

One of the most important results in this study is the participants' evaluation of sneezing frequency before and after the application of pollen therapy. We recorded statistically significant improvement in symptoms of our participants by the numeric score tests and these results provided the objective insight into the effectiveness of pollen therapy. We also obtained significant confirmation about fewer symptoms
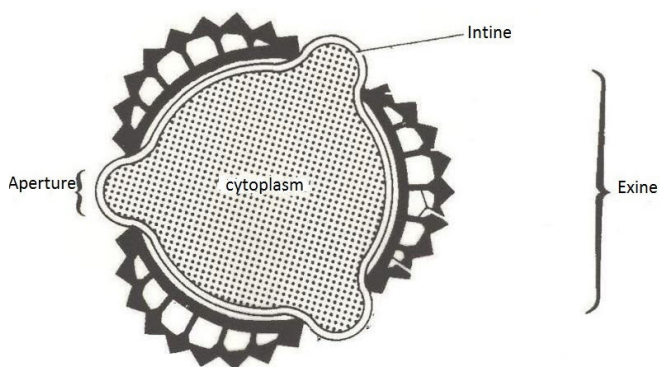

Figure 4. Pollen grain. Intine or inside layer is a thin and continuous layer made of cellulose or hemicellulose and pectin; Exine or outer layer is a highly decay-resistant chemical called sporopollenin; Apertures are areas on the walls of a pollen grain, where the wall is thinner and/or softer; Cytoplasm is the central part source of nuclei responsible for fertilization (19).

after pollen therapy from patients suffering from asthma and atopic problems.

Several participants experienced an improvement in symptoms of diseases (such as gastritis, arteriosclerosis, prostatic hyperplasia…) during the honey bee pollen treatment. Pollen treatment may lead to a systematic reduction of inflammations, but we are not able to confirm this as a direct cause without more detailed, hypothesis-driven research and experiments.

I would especially like to highlight the case of one of the participants, Patient #XX, who suffers from chronic anemia with a very weak immune status. Eight years prior to participation in this study, this participant was diagnosed with dysfunction of the thyroid gland and anemia. Although this participant took the required medicine, hemoglobin levels never exceeded 85g/L. Several years later, as a result of infectious endocarditis of the aorta´s valve, this participant had a brain hemorrhage with left-side paralysis. Two months after the brain hemorrhage, the patient received an artificial valve, and, as a result of long-term treatment, developed enterocolitis. Being familiar with my research and in agreement with their doctor, this patient decided to participate in this study. In addition to pollen therapy that all participants received, Patient #XX took 10 drops of propolis 3 times a day.

We noted several good factors in this case. This participant's complete blood count (CBC) improved, cholesterol level decreased, the symptoms of enterocolitis were significantly reduced, anticoagulant therapy was reduced to a minimum, and the general state of the participant's health was much better. Of course, throughout the study, this participant maintained their regular therapy, a combination of medications needed to treat existing conditions. Therapy in the form of iron, which this participant took for months before propolis, did not show a significant improvement in complete blood count. Only after the start of the treatment with the pollen, Patient #XX's hemoglobin levels significantly improved, monitored via laboratory blood tests once a week (Figure 3).

The pollen is one of the rare natural products that cannot be produced artificially in the laboratory due to its complex composition, and it contains substances mandatory for normal functioning and growth and development of the human body: proteins, fats, carbon hydrates, vitamins, minerals, enzymes, and hormones. It is richer in albumins than any other animal source, and it contains a higher content of the amino acids than the same quantity of beef, eggs, or cheese. Due to the high content of lecithin, the amino acids from pollen have favorable effects on body weight regulation, and it corrects biochemical disorders in the metabolism resulting in body weight correction.

We believe that our research points out that medicine for common diseases can be found in nature and that natural products such as pollen should be considered as an alternative to modern medicine. Although our research was limited by the lack of an untreated control or placebo group, we believe

Figure 5. Honey bee pollen – dry. Fresh pollen typically contains 10% to 12% water, while the moisture content of dried pollen is around four percent. Pure bee pollen for human consumption comes in granules.

Test	Value	Critical value	p-value
Anova	F=38.9	F = 3.958	0.000
Chi-squared	X^2 = 139.47	X^2 = 11.07	0.000
Matched pairs T-test	t = 2.02	t = 1.679	0.000

Table 2. Overview of statistical tests. The data collected was analyzed using a single factor (total symptoms score) ANOVA and Chi-squared test. T-test was used to determine the significance of differences between the total symptoms scores before (3.6) and after (2.2) pollen treatment. For all comparisons, p-value < 0.05 was considered statistically significant.

that it provides detailed and sufficient evidence that the honey bee pollen helps in treating allergic rhinitis. Results from this experiment give us guidance for numerous health issues that can be treated with honey bee pollen. In the future, we hope to further examine the relationship between pollen therapy and the treatment of other inflammatory diseases such as gastritis and arteriosclerosis.

MATERIALS AND METHODS

Before consuming, the pollen was dissolved in the water for several hours to make the grains swell. After this, the membrane cracks and releases useful substances. The human digestive system is not able to break this membrane; therefore, the pollen intake has no purpose unless it is dissolved in the water (Figure 4) (Figure 5).

All participants, including family members of the author, were familiarized with the treatment mode by the beekeeper, and then they have signed their consent to participate in the examination. All participants started with ¼ teaspoon (2g) per day and gradually worked their way up to 2 teaspoons (15g) at the end of the sixth week. Intake was gradually increased by a few grains every other day so that the maximal dose of 2 teaspoons was reached in 15 days. The maximal dose was then consumed for 30 consecutive days. All participants consumed the same amount of pollen. Participants usually took their dose with breakfast.

Participants filled in the questionnaire and on the visual analogous scale determined the level of symptoms and difficulties according to their individual as follows: 1 - No daily sneezing, 2 - Sneezing once per day, 3 - Sneezing several times per day, 4 - Often sneezing that does not disturb daily activities, 5 - Often sneezing that disturbs daily activities and 6 - Disturbing sneezing during the day. After the pollen application, participants filled in the questionnaire and on the same visual analogous scale determined the level of symptoms and difficulties according to their estimate. The questionnaire was compiled for this research and included visual analogous scales for estimation of sneezing and other complications, before and after the pollen application, including questions about the kind and intensity of sneezing, the quality of life, and allergic rhinitis.

All of the tests were done with the significance level of 5% and the null hypothesis (H0) was that the use of pollen does not reduce the problems caused by allergic rhinitis (Table 2). Based on test results, we reject H0 and conclude that intake of pollen reduces problems caused by allergic rhinitis.
The results of the questionnaire were analyzed using ANOVA, Chi-squared, and T-test. All tests were done using Microsoft Excel.

REFERENCES

1. Petković,Velina et al. "Senzibilizacija na inhalatorne alergene kod pacijenata sa alergijskim rinitisom." Medicinski časopis, vol. 45, no. 4, Srpsko lekarsko društvo, Okružna podružnica Kragujevac, 2011, pp. 21-26.
2. Blagojevic, Daniel. Alergija brošura. Austrijska Unija za pluća (ÖsterreichischeLungenunion), Beč, www.bencard.com/fileadmin/pdf/Patientenbroschueren/Allergiebroschuere_serbokroatisch.pdf
3. Poje, Gorazd, and Branica, Srećko. "Smjernice za liječenje alergijskog rinitisa – uloga intranazalnih kortikosteroida." Medicus, vol. 22, no. 2, Pliva Hrvatska d.o.o., Zagreb, 2013, pp. 90-91.
4. Marković, Snežana. Imunološki sistem čoveka. Institut za biologiju i ekologiju, Prirodno-matematički fakultet Univerziteta u Kragujevcu, 2013.
5. Maksimović, Nataša et al. "Kvalitet života obolelih od alergijskog rinitisa i bronhijalne astme." Vojnosanitetski

Pregled, Vol. 62, no. 4, Vojnomedicinska akademija – Institut za naučne informacije, Beograd, 2005, pp. 301-306.

6. Poje, Gorazd, and Branica, Srećko. "Smjernice za liječenje alergijskog rinitisa – uloga intranazalnih kortikosteroida." Medicus, vol. 22, no. 2, Pliva Hrvatska d.o.o., Zagreb, 2013, pp. 92-94.

7. Dizdarević, Zehra et al. "Alergijski rinitis." Clinical Immunology/Klinička imunologija, Edition: Ist, Chapter: 20, edited by Hajrija Seleskovć et al. Svjetlost Sarajevo, January 2007, pp. 393-412.

8. Bousquet, Jean et al. "Allergic rhinitis and its impact on asthma." J Allergy Clin Immunol, Vol 108, no. 5, Supplement, Nov. 2001, pp. 147-334.

9. "Apitherapy." Gale Encyclopedia of Alternative Medicine, Encyclopedia.com, www.encyclopedia.com/medicine/encyclopedias-almanacs-transcripts-and-maps/apitherapy

10. Marković, Aleksandar. Pčelinji proizvodi – eliksir zdravlja. 14 Sept. 2009, www.stetoskop.info/pravilna-ishrana/pcelinji-proizvodi--eliksir-zdravlja.

11. Paul, M. Ian et al. „"Effect of honey, dextromethorphan, and no treatment on nocturnal cough and sleep quality for coughing children and their parents." Arch Pediatr Adolesc Med., Vol. 161, no. 12, American Medical Association, USA, 2007, pp. 1140–1146.

12. Ashkin, Evan and Mounsey, Anne. "A spoonful of honey helps a coughing child sleep." Journal of Family Practice, Vol. 62, no. 3, American Academy of Family Physicians; Society of Teachers of Family Medicine; North American Primary Care Research Group; Association of Departments of Family Medicine, USA, 2013, pp. 145–147.

13. Miceli, Sopo S. et al. "Effect of multiple honey doses on non-specific acute cough in children. An open randomised study and literature review." Allergol Immunopathol (Madr), Volume 43, Issue 5, September–October 2015, pp. 449-455.

14. Mačukanović Jocić, Marina. Biologija medonosnog bilja sa atlasom apiflore Srbije. Poljoprivredni fakultet, Beograd, 2010. http://www.agrif.bg.ac.rs/files/uvid-javnosti/dr%20Marina%20Macukanovic%20Jocic%20Izvestaj.pdf

15. Bogdanov, Stefan et al. "Honey for Nutrition and Health: A Review." Journal of the American College of Nutrition, Volume 27, Issue 6, 2008, pp. 677-689.

16. Abadžić, Nijaz. Pčele za zdravlje. Advaita, Beograd – Sarajevo, 2016.

17. LInskens, H.F. and Jorde, W. "Pollen as food and medicine-A review." Economic Botany, Vol. 51, Article no. 78, The New York Botanical Garden, USA, 1997, pp. 78-86.

18. Kostić, Aleksandar, Analiza hemijskih i nutritivnih karakteristika polena koji su medonosne pčele sakupile u različitim regionima Srbije – Doktorska disertacija. Hemijski fakultet u Beogradu, Beograd, 2015.

19. Levaković, Marijana. Pelud – ljekovita svojstva i primjena – diplomski rad. Sveučilište Josipa Jurja Strossmayera u Osijeku, Fakultet agrobiotehničkih znanosti Osijek, Zavod za Lovstvo, Ribarstvo i Pčelarstvo, Zagreb, 2014, pp. 4-14.

20. Asha'ari, Zamzil Amin et al. "Ingestion of honey improves the symptoms of allergic rhinitis: evidence from a randomized placebo-controlled trial in the East coast of Peninsular Malaysia." Ann Saudi Med. Volume 33, Issue 5, September-October 2013, pp. 469-475.

21. Vezmar, Sandra and Miljković, Branislava. "Koncept farmaceutske zdravstvene zaštite i primena u alergiji." Bilten V simpozijuma farmaceutske komore Republike Srpske, Farmaceutska komora Republike Srpske, Banja Luka, 2008, pp. 40-51.

22. Laforest, Laurent et al. "Dispensing of antibiotics, antitussives and mucolytics to asthma patients: a pharmacy-based observational survey." Respir Med. 102(1), Jan 2008, pp. 57-63.

23. Ashkin, Evan and Mounsey, Anne. "A spoonful of honey helps a coughing child sleep." Journal of Family Practice, Vol. 62, no. 3, American Academy of Family Physicians; Society of Teachers of Family Medicine; North American Primary Care Research Group; Association of Departments of Family Medicine, USA, 2013, pp. 145–147.

Using graphene oxide to efficiently filter particulate matter at high concentrations

Yen-Ting Kuo[1], Huan-Tsung Chang[2]
[1] Taipei Fuhsing Private School, Taipei City, Taiwan
[2] National Taiwan University, Taipei City, Taiwan

SUMMARY

Air pollution is currently one of the biggest environmental challenges around the world. Air pollution not only causes detrimental effects to the human body but also endangers the natural environment. Many have proposed and created various methods to solve this problem, but none of them have worked very effectively. Following the discovery of graphene, scientists began to apply the use of this carbon material to address different kinds of problems. Using graphene oxide to combat air pollution, we prepared graphene oxide, which we then spread onto a commercial air filter, and used this air filter to purify air polluted with particulate matter (PM) of various diameters (PM_{10}, $PM_{2.5}$, or $PM_{1.0}$). We observed that filters with the addition of graphene oxide were able to purify polluted air containing PM at concentrations above $3000\ \mu g/m^3$, a concentration above which commercially available filters cannot. The efficiency of graphene oxide-treated filters was much greater than commercially available filters. Based on our data, we proposed a mechanism by which graphene oxide can effectively diminish the amount of PM in the air.

INTRODUCTION

Graphene oxide is a two-dimensional single layer of graphite, a continuous carbon structure with a thickness of 0.34. Graphene oxide is arranged in hexagonal patterns with functional groups attached to the carbon structure (1). Graphene oxide has many unique physical and chemical properties, compared to other allotropes of carbon and metals. For example, graphene oxide has properties such as high conductivity, high transparency, and high carrier mobility (2). Additionally, because of its high surface area to volume ratio, graphene oxide is considered as a potentially useful material in many different fields. For example, graphene oxide can replace silicon in the manufacturing of semi-conductors, it can be used in making cell phone or solar cell batteries, and it is even being considered in the development of potential cancer therapies (2). Of interest to our group, we explored the application of graphene oxide in air purification. Specifically, we prepared highly purified graphene oxide and investigated its efficiency in purifying polluted air, comparing graphene-oxide treated filters to commercially available air filters.

Particular matter (PM) is defined as particles that float in

the air. PM comprises most of the air pollution around the world and is separated into three categories according to particle diameter. $PM_{1.0}$ describes particles with a diameter of 1 mm and smaller, $PM_{2.5}$ describes particulates with a diameter of 2.5 mm and smaller, and PM_{10} describes particulates with a diameter of 10 mm and smaller. $PM_{2.5}$ is especially notable for its toxicity to the human body (3). In this paper, we showed that coating graphene oxide onto commercial filters increased the purification efficiency of air filters.

RESULTS

In this study, we investigated whether graphene oxide-treated air filters were more effective than commercially available filters in terms of purifying PM. First, using electrochemistry, we extracted and purified graphene oxide from used batteries. In order to confirm the identity and purity, we analyzed our graphene oxide sample using UV-Vis spectroscopy. We found that our extracted graphene oxide had almost the same peak absorption wavelength as previously reported for pure graphene oxide (**Figure 1**), confirming that our extracted graphene oxide had the expected properties of a relatively pure sample (4).

We first tested a set of controls: We used no filter, a commercial filter, and an activated carbon filter. We picked the commercial filter and the activated carbon since they are commercially available and commonly used. Notably, activat-
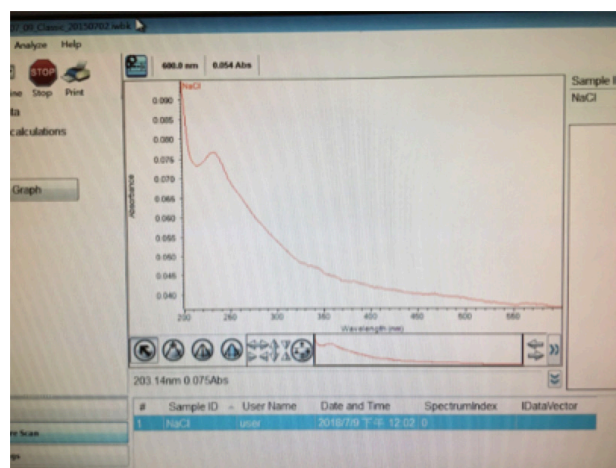

Figure 1. The UV-Vis spectrum of extracted graphene oxide sample. After extracting carbon rods from used batteries and purifying graphene oxide using electrochemistry, the purity of graphene oxide was confirmed using UV-Vis spectroscopy.
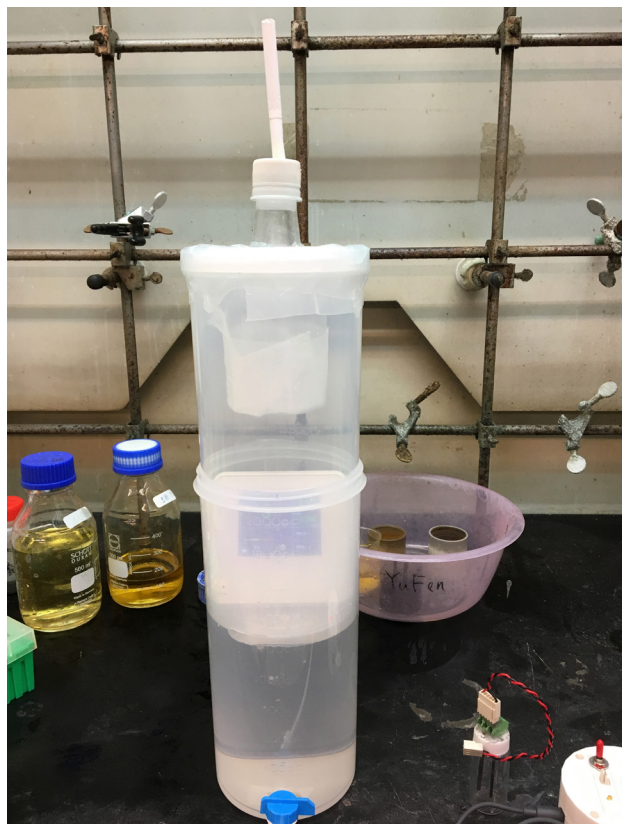
Figure 2. Experimental model. The setup was a simplified model of the human lung, consisting of several stacked chambers. When the cigarette at the top of the model was lit, air within the chamber was polluted with particulate matter (PM). As water at the bottom of the chamber was released, air was pulled from the top of the chamber, through the experimental filter, and reached the PM detector.

ed carbon and graphene oxide groups differ in particle size, since one particle of activated carbon is about 1000 times larger than that of graphene oxide. This leads to different filter spaces and may lead to differing performance. Of our experimental groups, we decided to test seven groups of commercial filters coated with differing concentrations of graphene oxide. We used 2 mg of graphene oxide dissolved in different volumes (50, 75, 100, 125, 150, 200 mL) of ethanol, to determine which group had the highest purification efficiency.

To test the purification efficiency of different filters, we built an experimental model in which we tested each filter's ability to purify PM from a cigarette (**Figure 2**). Our experimental setup was designed as a model of the lung. Water serves the function of a diaphragm in our model, because as the water flows out of the container (diaphragmatic contraction), the volume of the "empty" container (lung) becomes larger. As a result, air then flows into the chamber. In our experiment, we allowed water to flow out of the container after we lit a cigarette at the top of the experimental chamber. As the water flowed out of the chamber, air flowed through the cigarette smoke, pulling filtrate into the experimental filters. We measured the time it took for $PM_{2.5}$ within the model to reach 250 ug/m³, the concentration considered to be hazardous to human life. The

control, activated carbon, and untreated filter conditions took 50, 100, and 115 seconds, respectively, to reach 250 ug/m³. In the graphene oxide-coated filter groups, it took about 90-280 seconds to reach this point (**Figure 3, Figure 4**)However, the 2 mg graphene oxide per 100 mL ethanol group had the longest latency period before the $PM_{2.5}$ concentration reached 250 g/m³, taking the longest time of about 500 seconds.

Next, we compared the purification efficiency of filters treated with different graphene oxide concentrations, across different categories of PM. Specifically, we calculated both the purification efficiency and breakthrough time of the control and experimental groups (**Table 1**). In this experiment we concluded that the filters treated with 2 mg graphene oxide per 100 mL ethanol had the highest purification efficiency (**Figure 5**).

We also calculated the filter capacity, defined as the amount of PM held by a filter. We were interested in measuring how much more PM could be held by graphene-oxide coated filters than commercially available filters. We found that the filters treated with 2 mg graphene oxide per 100 mL ethanol had the biggest filter capacity of about 29 g/m³ (**Figure 6**).

DISCUSSION

In our study, we hoped to create a filter that could address the problem of air pollution. We focused on removing PM, because PM is the main source of air pollution and has many detrimental effects on the environment. We aimed to capture an effective amount of PM in a given amount of time, supporting that removal of PM using our methods could become a good solution in tackling the current global problem of air pollution.

In our experiments, we coated air filters with different concentrations of graphene oxide in ethanol and tested their purification efficiencies. Across the different concentrations of graphene oxide, we found that all concentrations of treatment were able to purify PM more effectively than commercially available filters. Specifically, we discovered that filters treated with 2 mg graphene oxide per 100 mL ethanol had the longest
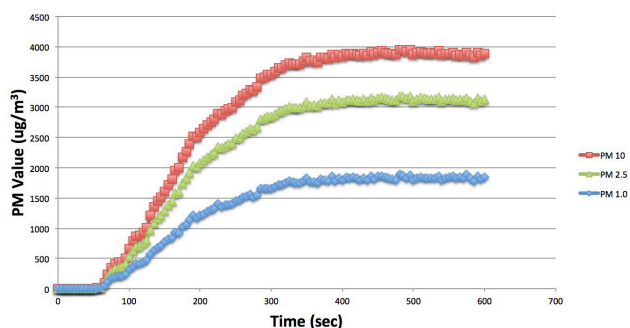

Figure 3. Concentrations of particulate matter over time following filtration using activated carbon filters. As a control experiment, an activated carbon filter was placed in the chamber under the cigarette. After lighting the cigarette and releasing water out of the chamber, allowing air to flow, the PM detector measured concentrations of PM with diameters of 1.0, 2.5, or 10 micrometers and less.
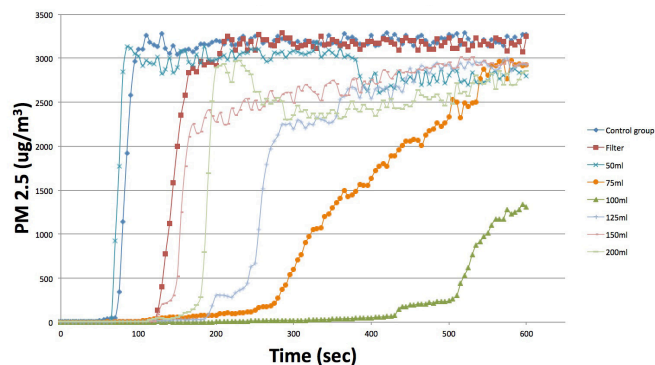
Figure 4. Concentrations of PM$_{2.5}$ over time following filtration using filters coated with different concentrations of graphene oxide. The PM detector was used to measure PM2.5 over time after the cigarette was lit and air was pulled through either no filter (control), a commercial air filter, or a filter coated with 2 mg of graphene oxide powder resuspended in various volumes of ethanol.

Purification Efficiency (%)	PM 1.0	PM 2.5	PM 10	PM 2.5 Breakthrough (250 ug/m3) Time
Control Group	N/A	N/A	N/A	50 Seconds
Commercial Filter (3M Filters)	95.56%	95.91%	95.75%	115 Seconds
Activated Carbon	97.55%	97.56%	97.57%	100 Seconds
2 mg Graphene Oxide/50 ml Ethanol	98.76%	98.83%	98.81%	90 Seconds
2 mg Graphene Oxide/ 75 ml Ethanol	99.88%	99.83%	99.83%	278 Seconds
2 mg Graphene Oxide/ 100 ml Ethanol	99.92%	99.96%	99.96%	502 Seconds
2 mg Graphene Oxide/ 125 ml Ethanol	99.82%	99.83%	99.8%	198 Seconds
2 mg Graphene Oxide/ 150 ml Ethanol	99.88%	99.83%	99.83%	141 Seconds
2 mg Graphene Oxide/ 200 ml Ethanol	99.76%	99.66%	99.65%	178 Seconds

Table 1. Purification efficiencies and breakthrough times of control and experimental groups. Values of purification efficiencies were reported for various tested filters across different categories of PM. Breakthrough time was calculated as the time required for the concentration of PM with a diameter of 2.5 micrometers or less to reach 250 ug/m^3.

breakthrough time, highest purification efficiency, and largest filter capacity of all other filters. Due to the surprising results of the 2 mg graphene oxide per 100 mL ethanol treatment, we decided to investigate the mechanisms that may have helped shape this purification effect. We came up with three possibilities to explain why the 2 mg graphene oxide per 100 mL ethanol group had the highest purification efficiency when compared to the other graphene oxide-coated filters.

First, the 2 mg graphene oxide per 100 mL ethanol group might have had the most even spread of graphene oxide over the filter. Secondly, graphene oxide contains several functional groups, such as hydroxyl and carboxyl groups, which could interact with polar PM molecules (1). Thirdly, the coated filter may have acted by using electrostatic adhesion to filter particles (1). However, more research should be done, perhaps through micro-structure analysis, to more fully investigate the reason why 2 mg graphene oxide per 100 mL ethanol had the highest efficiency.

In addition, we calculated the breakthrough time, defined as the time it took to reach a PM$_{2.5}$ concentration of of 250/ for all the graphene oxide-coated groups. We found that the 2 mg graphene oxide per 100 mL ethanol group had the longest breakthrough time, at about 500 seconds. Also, we calculated the filter capacity, defined as the amount of PM that graphene oxide-coated filters can hold, compared to commercially available filters. We found that the 2 mg graphene oxide per 100 mL ethanol group had the largest filter capacity of 29 g/m^3.

In our experiments, we concluded three main points to summarize the results of this experiment and highlight future directions. First, we successfully obtained graphene oxide powder using electrochemistry and measured purity with UV-Vis technology. Secondly, we determined that graphene oxide-modified filters had a higher purification efficiency, compared to a representative commercial filter. Moreover, the filter modified with 2 mg graphene oxide per 100 mL ethanol had the highest purification efficiency. In the future, we propose changing the organic solvent and experimental parameters to make further improvements on the purification

process, and we will compare our filters to HEPA filters, filters that are designed by NASA to purify polluted air with an ability to filter 99.97% of the air particles with a diameter above 3. Additionally, in later experiments, we propose using micro-structure analysis to investigate the mechanism of air purification. Also, we will use organic solvents such as acetone because, while acetone serves similar functions as ethanol, it might produce different results since the chemical structure does not contain as many hydroxyl groups as that of ethanol (5). In addition, we will more definitively characterize the properties of our purified graphene oxide by analyzing any unexpected changes in carbon form or structure after being purified via electrochemistry.

Finally, we hope to find solutions that will help remove particulate matter from the filter, focusing on removing carbon
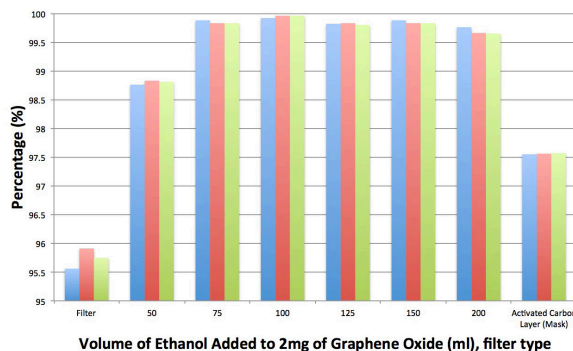

Figure 5. Purification efficiencies of different graphene oxide concentrations. The PM detector was used to measure concentrations of PM of different diameters. The filters tested were a commercial filter, an activated carbon filter, and filters coated with 2 mg of graphene oxide powder resuspended in various volumes of ethanol. Comparing the activity of each filter compared to no filter, purification efficiencies were calculated.
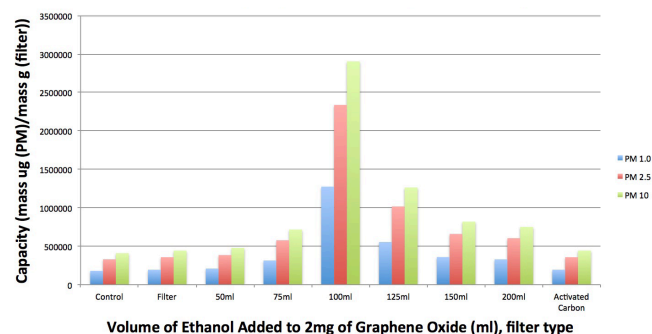
Figure 6. Filter capacities of different graphene oxide concentrations. The PM detector was used to measure concentrations of PM of different diameters. The filters tested were a commercial filter, an activated carbon filter, an uncoated filter, or a filter coated with 2 mg of graphene oxide powder resuspended in various volumes of ethanol. The filter capacities were calculated based on the saturated PM concentration of the control group.

monoxide since it takes up most of the chemical composition percentage in a cigarette, to make the filter reusable (6). This solution might help wash off PM on the filter and make the filter clean again. Because of this, a filter can be reused many times. With high purification efficiency and high reusability, coated filters are a potentially promising solution to addressing the world's air pollution problem.

MATERIALS AND METHODS
Purification of nano-graphene oxide

We used electrochemistry (4) to obtain highly purified nano-graphene oxide. We extracted carbon rods from used batteries (Panasonic NEO AA type battery), using 1 M sodium chloride as the aqueous solution and put two carbon rods in the solution. Next, we applied 10 Volts to the solution using a voltmeter for 1 hour. After electrolysis, we centrifuged the aqueous solution at 25000 RPM (rotations per minute) for 15 minutes, three times. After centrifugation, we incubated the solution for 1 day before testing its purity via UV-Vis spectroscopy. After testing its purity, the solution was lyophilized in the shelf freeze dryer to remove water for three to four days, resulting in with samples of graphene oxide power.

Applying graphene oxide to a filter

After extracting the graphene oxide powder, we mixed 2 mg of powder with different volumes (50, 75, 100, 125, 150, 200 mL) of ethanol by sonication, making sure that the powder was dispersed throughout the solution. Then, we put a 3M filter inside a petri dish and spread the graphene oxide/ethanol solution evenly onto the filter using a dropper. Next, we put the petri dish into an incubator at 60°C to separate the ethanol and graphene oxide.

Testing removal of particulate matter

At the top of our setup, we used a cigarette as the pollution source (Figure 2). Underneath that was our experimental filter to filter the polluted air. Below the filter was the PM detector, which can detect the concentrations of $PM_{1.0}$, $PM_{2.5}$, and PM_{10}

of filtered air in order to measure the purification efficiency of each filter. At the bottom of the setup, we installed a water opening to let the water flow out of the container, in order to pull the air down so the polluted air could be filtered by the experimental filter at a steady rate.

After the experiment, we measured the efficiency of a filter by using the following equation:

$$Efficiency = 100 - \left(\frac{Particles\ allowed\ through\ filter}{Particles\ allowed\ through\ with\ no\ filter} \times 100 \right)$$

Lastly, we also calculated the filter capacity of all the tested groups. In this case, we use the formula:

$$Filter\ Capacity \left(\frac{mass(PM)}{mass(filter)} \right) =$$

$$PM\ concentration\ rising\ time\ (seconds) * Flowrate \left(\frac{1000ml}{600s} \right) *$$

$$Saturated\ PM\ Concentration\ of\ control\ group\ (\mu g/m^3)$$

REFERENCES
1. "Graphene Oxide." *Graphene Oxide - an Overview | ScienceDirect Topics*, www.sciencedirect.com/topics/materials-science/graphene-oxide.
2. "Graphene applications: what is graphene used for?" *Graphene*, 9 Dec. 2019, www.graphene-info.com/graphene-applications.
3. "Particulate Matter (PM) Basics." *EPA*, Environmental Protection Agency, 14 Nov. 2018, www.epa.gov/pm-pollution/particulate-matter-pm-basics.
4. Wazir, A H, and I W Kundi. "Synthesis of Graphene Nano Sheets by the Rapid Reduction of Electrochemically Exfoliated Graphene Oxide Induced by Microwaves." *Journal of the Chemical Society of Pakistan*, vol. 38, no. 1, 2016, pp. 11–16.
5. "Acetone." *National Center for Biotechnology Information. PubChem Compound Database*, U.S. National Library of Medicine, pubchem.ncbi.nlm.nih.gov/compound/Acetone.
6. Tayyarah, Rana, and Gerald A. Long. "Comparison of Select Analytes in Aerosol from e-Cigarettes with Smoke from Conventional Cigarettes and with Ambient Air." *Regulatory Toxicology and Pharmacology*, vol. 70, no. 3, 2014, pp. 704–710., doi:10.1016/j.yrtph.2014.10.010.

Sponsorship

Editor's Circle $10,000+

ALLOY THERAPEUTICS

Patron $5,000+

NEW ENGLAND BioLabs Inc.
enabling technologies in the life sciences

PORTFOLIOS WITH PURPOSE®

Institutional Supporters

HARVARD UNIVERSITY

HARVARD MEDICAL SCHOOL

Tufts UNIVERSITY 1852

Charitable Contributions

We need your help to provide mentorship to young scientists everywhere.

JEI is supported by an entirely volunteer staff, and over 90% of our funds go towards providing educational experiences for students. Our costs include manuscript management fees, web hosting, creation of STEM education resources for teachers, and local outreach programs at our affiliate universities. We provide these services to students and teachers entirely free of any cost, and rely on generous benefactors to support our programs.

A donation of $30 will sponsor one student's scientific mentorship, peer review and publication, a six month scientific experience that in one student's words, 're-energized my curiosity towards science', and 'gave me confidence that I could take an idea I had and turn it into something that I could put out into the world'. **If you would like to donate to JEI, please visit https://emerginginvestigators.org/support, or contact us at questions@emerginginvestigators.org.** Thank you for supporting the next generation of scientists!

'Journal of Emerging Investigators, Inc. is a Section 501(c)(3) public charity organization (EIN: 45-2206379). Your donation to JEI is tax-deductible. '